OXFORD

SOT | Society of Toxicology
www.toxsci.oxfordjournals.org

TOXICOLOGICAL SCIENCES, 149(1), 2016, 67–88

doi: 10.1093/toxsci/kfv214
Advance Access Publication Date: September 22, 2015
Research Article

Gene Expression Patterns Associated With Histopathology in Toxic Liver Fibrosis

Danielle L. Ippolito,*,[1] Mohamed Diwan M. AbdulHameed,[†] Gregory J. Tawa,[†,2] Christine E. Baer,[‡] Matthew G. Permenter,[‡] Bonna C. McDyre,[§] William E. Dennis,* Molly H. Boyle,[¶] Cheryl A. Hobbs,[¶] Michael A. Streicker,[¶] Bobbi S. Snowden,[||] John A. Lewis,* Anders Wallqvist,[†] and Jonathan D. Stallings*

*The Environmental Health Program, The United States Army Center for Environmental Health Research (USACEHR), Fort Detrick, Maryland 21702-5010; [†]Department of Defense Biotechnology High Performance Computing Software Applications Institute, Telemedicine and Advanced Technology Research Center, U.S. Army Medical Research and Materiel Command, Ft. Detrick, Maryland 21702; [‡]Excet, Inc. and [§]Oak Ridge Institute for Science and Education, Frederick, Maryland 21702-5010; [¶]Integrated Laboratory Systems, Research Triangle Park, North Carolina 27709; and [||]Maryland Institute for Applied Environmental Health, School of Public Health, University of Maryland, College Park, Maryland 20742

[1]To whom correspondence should be addressed at Biomarkers Program; U.S. Army Center for Environmental Health Research; 568 Doughten Drive; Fort Detrick, MD 21702-5010. Fax: (301) 619-7606. E-mail: Danielle.L.Ippolito2.civ@mail.mil.

[2]Present address: Translational Medicine Division, National Institutes of Health, Bethesda, MD.

Disclaimer: The studies producing this research were approved by the Institutional Animal Care and Use Committee, and research was conducted in compliance with the Animal Welfare Act, and other federal statutes and regulations relating to animals. Experiments involving animals adhered to principles stated in the *Guide for Care and Use of Laboratory Animals* as prepared by the Committee on Care and Use of Laboratory Animals of the Institute of Laboratory Animal Resources, National Research Council in facilities that are fully accredited by the Association for Assessment and Accreditation of Laboratory Animal Care, International.

ABSTRACT

Toxic industrial chemicals induce liver injury, which is difficult to diagnose without invasive procedures. Identifying indicators of end organ injury can complement exposure-based assays and improve predictive power. A multiplexed approach was used to experimentally evaluate a panel of 67 genes predicted to be associated with the fibrosis pathology by computationally mining DrugMatrix, a publicly available repository of gene microarray data. Five-day oral gavage studies in male Sprague Dawley rats dosed with varying concentrations of 3 fibrogenic compounds (allyl alcohol, carbon tetrachloride, and 4,4′-methylenedianiline) and 2 nonfibrogenic compounds (bromobenzene and dexamethasone) were conducted. Fibrosis was definitively diagnosed by histopathology. The 67-plex gene panel accurately diagnosed fibrosis in both microarray and multiplexed-gene expression assays. Necrosis and inflammatory infiltration were comorbid with fibrosis. ANOVA with contrasts identified that 51 of the 67 predicted genes were significantly associated with the fibrosis phenotype, with 24 of these specific to fibrosis alone. The protein product of the gene most strongly correlated with the fibrosis phenotype PCOLCE (Procollagen C-Endopeptidase Enhancer) was dose-dependently elevated in plasma from animals administered fibrogenic chemicals ($P < .05$). Semiquantitative global mass spectrometry analysis of the plasma identified an additional 5 protein products of the gene panel which increased after fibrogenic toxicant administration: fibronectin, ceruloplasmin, vitronectin, insulin-like growth factor binding protein, and α2-macroglobulin. These results support the data

mining approach for identifying gene and/or protein panels for assessing liver injury and may suggest bridging biomarkers for molecular mediators linked to histopathology.

Key words: toxic liver injury; transcriptomics; bioinformatics; fibrosis; biomarkers; histopathology

More than 84 000 chemicals are in existence around the globe with hundreds more introduced for consumer use each year (Allen, 2013). Given the expense and time required for animal-based toxicity profiling, most of these chemicals will never be adequately assessed for toxicity, and, hence, we need practical alternatives to the comprehensive testing paradigm. Complementary methods to predict end organ toxicity can provide an alternative measure of toxicological effects associated with chemical hazards. Advances in data mining strategies and the availability of large public repositories of toxicology data derived from thousands of chemical exposures have enabled advances in hypothesis-driven phenotypic linking of gene expression to pathological responses (Ganter *et al.*, 2005; Igarashi *et al.*, 2015; Ihmels *et al.*, 2002; National Toxicology Program, 2010). Mining these databases using bioinformatics or systems biology tools has the potential to elucidate molecular mechanisms of drug toxicity by linking gene expression profiles, toxicity pathways, and standard-of-care clinical testing parameters (Edginton and Willmann, 2008; Harrill and Rusyn, 2008). Thus, computational systems toxicology uses the concept of a toxicity-related biological pathway to identify sets of genes or proteins that can be incorporated in biomarker panels whose differential readout can then be linked to different chemical injuries. Termed "bridging biomarkers," these analytes are designed to link specific adverse effects, regardless of the nature of the chemical injury, to clinically relevant endpoints such as abnormal histopathology with better accuracy than any single analyte.

The liver is one of the primary organs affected by exposure to toxic industrial chemicals and pollutants due to its central role in xenobiotic metabolism (Antoine *et al.*, 2013). The heterogeneity in response among individuals to toxic chemicals and the multitude of pathways contributing to hepatic injury makes it unlikely that any single gene or biomolecule will be sufficient as an early indicator of hepatic injury (Aldridge *et al.*, 2003; Campion *et al.*, 2013). Multiplexed panels of biomolecules for hepatotoxicity will have greater applicability across a wide range of chemical-dose-exposure scenarios (Alfirevic and Pirmohamed, 2012; Meldrum *et al.*, 2011). Toxicogenomics holds promise for identifying changes in multiple genes induced by exposure to hepatotoxic chemicals (Amacher, 2010; Beger *et al.*, 2010; Fontana, 2014; Heinloth *et al.*, 2007). Importantly, mechanistic-based biomarker discovery provides an early recognition of signature gene changes reflecting a specific toxicological endpoint regardless of the original chemical insult (Ozer *et al.*, 2008).

Mining large repositories of publically available data affords insight into gene changes correlating with specific liver histopathologies (Cui and Paules, 2010; Heinloth *et al.*, 2007). One such resource is the DrugMatrix database (Ganter *et al.*, 2005; National Toxicology Program, 2010), a public repository of microarray data, histopathology, and clinical chemistry data from more than 3200 drug and toxicant exposures in Sprague Dawley rats. Of the chemicals tested in the repository, 127 are toxic industrial chemicals (ie, nonpharmaceuticals), with 1221 associated gene expression profiles, clinical chemistry data, and graded histology slides from liver toxicity endpoints. The repository is fertile ground for training computational algorithms predictive of liver pathology. In recent publications, we used data in the DrugMatrix database as a training data set to identify coexpression modules and protein-protein interaction (PPI) networks associated with pathogenesis of liver disease, with particular emphasis on liver fibrosis (AbdulHameed *et al.*, 2014; Tawa *et al.*, 2014).

In our previous work, we identified coexpression modules predictive of the liver fibrosis pathology by bioinformatically mining the DrugMatrix data repository (AbdulHameed *et al.*, 2014; Ihmels *et al.*, 2002; Tawa *et al.*, 2014). The purpose of this study was to (1) identify gene expression patterns phenotypically anchored to histopathology, (2) determine whether the protein products of genes coding for secreted proteins are differentially expressed in plasma, and (3) determine whether any of these genes are early indicators of fibrogenesis. To achieve these aims, we downselected the genes previously identified in the coexpression modules to a 67-plex panel and experimentally verified the robustness and reproducibility of the panel in diagnosing liver fibrosis. We tested the fidelity of the 67-plex signature in Sprague Dawley rats administered 5 compounds orally for 5 days (Table 1). All chemicals were also tested in the DrugMatrix studies. Three of the 5 chemicals were prototypic fibrotic agents with the remaining 2 chemicals known to induce nonfibrotic liver damage. The fibrogenic toxicants 4,4′-methylenedianiline (4,4′-MDA) (4,4′-diaminodiphenylmethane) and allyl alcohol independently caused microscopic evidence of bile duct hyperplasia and fibrosis comparable to the DrugMatrix studies. Carbon tetrachloride caused delayed-onset fibrosis in the DrugMatrix studies (ie, after 28-days of exposure), although our study identified evidence of increased centrilobular collagen at 5 days, which is indicative of early fibrotic lesions as previously described (Fujii *et al.*, 2010; Kamada *et al.*, 2003). The nonfibrogenic chemicals did not cause fibrosis, although both were hepatotoxic. Bromobenzene caused fatty liver and hepatic necrosis at high doses and dexamethasone caused microscopic evidence of glycogen accumulation and hepatic necrosis. Allyl alcohol and 4,4′-MDA administration resulted in a dose-dependent increase in differential gene expression commensurate with the fibrosis histopathology in 90%–95% of the gene signature panel. The results obtained in our microarray analysis and the previous DrugMatrix studies were independently verified using Bioplex technology with 76% of the signature genes exhibiting differential expression in animals presenting with fibrosis. These data demonstrate the utility of mining large repositories of experimental data using systems toxicology techniques to identify markers for specific histopathologies.

MATERIALS AND METHODS

Test chemicals. The following test chemicals were purchased from Sigma Aldrich Corporation (St Louis, Missouri): 4,4′-MDA ((chemical abstracts service)CAS No. 101-77-9), dexamethasone (CAS No. 50-02-2), allyl alcohol (CAS No. 107-18-6), bromobenzene (CAS No. 108-86-1), and carbon tetrachloride (CAS No. 56-23-5). All chemical compounds were diluted in corn oil (CAS No. 8001-30-7) (MP Biomedicals, LLC [Solon, Ohio]). The dose volume was 5 ml/kg. Doses were selected based on doses published in

TABLE 1. Compound-Dose Groups and Presumptive Mechanisms of Toxicity After Oral Exposure in Rats

Compound	Structure	Doses (mg/kg)	Mechanism of Hepatotoxicity	Predicted Histopathology
Fibrogenic:				
Allyl Alcohol [a,b,d]	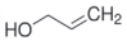	Group 1 (n=5): 0, 21, 27, 35, 45 Group 2 (n=4): 0, 5, 10, 21, 45	Free radical damage by toxic metabolite (acrolein): 	Fibrosis, bile duct hyperplasia
4,4'-Methylene-dianiline (MDA) [a,c,d]	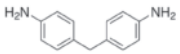	Group 1 (n=5): 0, 22, 60, 162 Group 2 (n=4): 0, 8, 22, 60, 162	Conversion to toxic metabolites by n-acetyl-transferase enzymes 	Fibrosis, necrosis, bile duct hyperplasia
Carbon tetrachloride [a,d,e]		Group 1 (n=5): 0, 20, 43, 93, 200 Group 2: 0, 200 (n=4)	Free radical damage by toxic metabolite, lipid peroxidation • CCl_3	Fatty liver, necrosis, fibrosis (delayed-onset)
Non-Fibrogenic:				
Bromobenzene [a,d]		Group 1 (n=5): 0, 124, 229, 424, 785 Group 2 (n=4): 0, 785	Free radical damage by toxic metabolite: 	Fatty liver, necrosis
Dexamethasone [a,d]	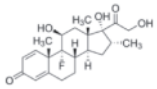	Group 1 (n=4): 0, 1 Group 2 (n=5): 0, 1	Indirect lipid accumulation by increased circulating triglycerides	Minimal; glycogen accumulation

Dose Selection: a, Ganter *et al.*, 2005; b, Irwin, 2006; c, National Toxicology Program, 2002; d, National Toxicology Program, 2010; e, National Toxicology Program, 2011; 5, Smialowicz *et al.*, 1991.

the DrugMatrix database, the National Toxicology Program reports, and Agency for Toxic Substances and Disease Registry reports (Ganter *et al.*, 2005; Irwin, 2006; National Toxicology Program, 2002, 2010, 2011; Smialowicz *et al.*, 1991).

Animals. *In vivo* rat experiments were performed at Integrated Laboratory Systems (ILS, Research Triangle Park, North Carolina). The ILS Institutional Animal Care and Use Committee approved all experimental procedures. Research was conducted in compliance with the Animal Welfare Act, and other federal statutes and regulations relating to animals. Experiments involving animals adhered to principles stated in the *Guide for Care and Use of Laboratory Animals* (Institute of Laboratory Animal Resources, 2011) as prepared by the Committee on Care and Use of Laboratory Animals of the Institute of Laboratory Animal Resources, National Research Council in facilities that are fully accredited by the Association for Assessment and Accreditation of Laboratory Animal Care, International. Male Sprague Dawley rats (CD IGS [CRL:CD (SD)]) were purchased from Charles River Laboratories (Raleigh, North Carolina). Rats weighing 215–245 g (8 weeks old) were used. Briefly, rats were housed 2 per cage with a rat tunnel enrichment device (Bio-Serve, Frenchtown, New Jersey). Rats were fed a Purina Rodent Diet No. 5002 (Ralston Purina Co, St Louis, Missouri), supplied *ad libitum*. Animals received reverse osmosis-treated tap water (City of Durham, North Carolina) *ad libitum*, which was changed at least once weekly. Controls in the animal rooms were set to maintain temperatures between 20°C–25°C with a relative humidity of 30%–70% and a 12-h light/12-h dark cycle, lights on at 6:00 AM. Clinically healthy animals were assigned to dose groups using a procedure that stratifies animals across groups by body weight such that mean body weight of each group was not statistically different from any other group using ANOVA (Statistical Analysis System version 9.2, SAS Institute, Cary, North Carolina). Animals were dosed by oral gavage for 5 consecutive days (± 10 min) from the previous day's dose administration time) (Table 1). Volume was based upon daily body weight. Two separate groups of experimental animals were used in the analysis: the training set (group 1, processed for microarray analysis) and the testing set(group 2, processed for Bioplex analysis).

Clinical observations and tissue collection. Animals were observed cage-side 1 h following daily dose administration, then 1–2 times per day during dosing regimens. Body weights were measured daily prior to dose administration, and prior to euthanasia. Twenty-four hours after the final dose administration, animals were euthanized. Livers were harvested at necropsy and weighed to within 0.1 g. One-half of the left lobe of the liver was fixed in 10% formalin. The remaining half of the left lobe of the liver was flash frozen in liquid nitrogen, then stored below −70°C. Liver specimens were frozen in < 3 min from time of death.

Histopathology. Formalin-fixed liver specimens were embedded in paraffin blocks. A 5-μm section of liver from each animal was stained with hematoxylin and eosin, Oil Red O, and Masson's trichrome for microscopic evaluation. The tissues were evaluated by a pathologist certified by the American College of Veterinary Pathologists (MHB). Tissues were semiquantitatively and qualitatively scored for degree of pathology on a descriptive scale with the following distribution: None, 0% of tissue affected; Minimal, > 0%–30% of tissue affected; Mild, > 30%–60% of the tissue affected; Moderate, 60%–80% of the tissue affected; Marked, > 80% of the tissue affected.

RNA isolation. Working on dry ice, a portion (approximately 10 mg) of flash-frozen liver was cut from each sample and transferred to a clean, labeled tube. Total RNA was then isolated using Qiagen's miRNeasy 96 kit (Qiagen, Valencia, California) following manufacturer's instructions with a final elution volume of approximately 150 µl (2 × 75 µl). The quality and quantity of RNA samples were evaluated with a 2100 Bioanalyzer (Agilent Technologies, Santa Clara, California), using the Agilent RNA 6000 Nano Reagents and a multiwell NanoDrop 8000 spectrophotometer (Thermo Fisher Scientific, Waltham, Massachusetts).

Transcriptomics analysis: Affymetrix gene array. Hybridization-ready, fragmented, labeled, sense-stranded DNA targets were prepared using Affymetrix GeneChip WT Plus Reagent Kit (Affymetrix, Santa Clara, California) according to manufacturer's recommendations with an input of 100 ng total RNA. The labeled cDNA targets, trays, and arrays were prepared with the GeneTitan Hybridization, Wash and Stain Kit for WT array plates (Affymetrix). Samples were applied to the Rat Gene 2.1 ST 96 Array Plate and analyzed in the GeneTitan System (Affymetrix) according manufacturer's recommendations. GeneTitan scanning quality control was performed, including visual inspection and quality control metrics supplied by Expression Console (ie, hybridization control performance, labeling control performance, internal control gene performance, signal histogram, probe cell intensity, Pearson's Correlation and Spearman Rank Correlation, and Affymetrix). Pearson's R^2 was calculated for each set of replicates within each group. Replicates not meeting these criteria were repeated (threshold: R^2 of 85%).

Gene array data analysis. The arrays were normalized using an extension of the Probe Logarithmic Intensity Error (PLIER) algorithm (ie, the iterPLIER procedure in the Affymetrix Expression Console). The gene level iterPLIER procedure discards poor-performance feature sets, (Qu *et al.*, 2010). ".CHP" files were imported into Partek Genomics Suite (version 6.12.0907). Affymetrix library files included all available reference files related to RaGene-2_1-st. An ANOVA using pathologies as variables was conducted with contrasts to determine differentially expressed genes with an (false discovery rate) FDR < 0.05 by Benjamini-Hochberg False Discovery Rate (Qu *et al.*, 2010; Reiner *et al.*, 2003).

Microarray data described in this study have been deposited in the Gene Expression Omnibus database with accession number GSE70559.

iTRAQ (isobaric tag for relative and absolute quantification) analysis. Serum and plasma proteins were immunodepleted using the Agilent Multiple Affinity Removal System (MARS) for Human-14 column and Thermo Seppro 7 spin column for rat. For the Thermo Seppro 7 spin column (PN S6199), 20 µL of serum or plasma were depleted according to the manufacturer's instructions. For the MARS depletion, 50 µl of sample was diluted with 450 µl of Agilent Buffer A (PN 5185-5987) and filtered through Agilent 0.22 µM spin filters (PN 5185-5990). To prevent overloading the column, 2 injections of 200 µl each were made onto an Agilent HU-14 4.6 × 100 mm column (PN 5188-5218) maintained at 23°C. An Agilent 1100 HPLC equipped with an autosampler with an expanded injection loop and needle seat, a diode array detector, a fraction collector, and a Chemstation data system was used for the separation. The sample well plate and fraction collector was set to 8°C. A gradient was used for the separation. The initial conditions were 100% buffer A at a flow rate of 0.5 ml/min. The initial conditions were maintained for 15 min. At 15.01 min the solvent was changed to 100% Buffer B (Agilent PN 5185-5988) and the flow rate was increased to 1 ml/min. These conditions were maintained until 22 min, and then a gradient to 100% Buffer A at 1 ml/min was completed at 22.1 min. At 33 min, the flow rate was reduced to 0.25 ml/min and the run was stopped. The 280 nm wavelength was monitored to ensure the reproducibility of the injections. The fraction collector was programmed to collect time-based 1 min fractions starting at 2 min and was turned off at 18.9 min. Fractions 1 through 12 from both injections were pooled from to create the flow-through "F1" fraction.

The depleted samples were buffer exchanged using Agilent 5 kDa molecular weight cut off filters. The flow-through fraction was reduced to < 500 µl by centrifugation. Three milliliters of 10 mM tetraethylammonium bicarbonate were added and the sample reduced to 500 µl. This step was repeated twice. On the final spin, the sample was reduced to 300 µl or less. The final volume was brought back to 300 µl, filtered through Agilent spin filters, and protein concentration was determined using Pierce BCA assay (PN 23227, Thermo Scientific, Rockford, lL). For iTRAQ labeling, all of the protein and reagents were doubled to increase the amount of protein injected. Two hundred micrograms of the protein was dried by speed vaporator and treated to the iTRAQ protocol using iTRAQ 8-plex reagents (PN 4390812, Sciex, Redwood City, California). Samples were reduced in 50 mM tris-(2-carboxyethyl) phosphine; cysteines were blocked in 200 mM methanethiosulfonate; and proteins were digested with 10 µg trypsin overnight and then isotopically labeled. The combined iTRAQ samples were then put in a vacuum centrifuge for 2 h at 45°C to remove the majority of the isopropanol. One thousand one hundred microliters of mobile phase was added to the sample (3% formic acid: 2 mM ammonium formate: 25% acetonitrile in water).

Samples were fractionated using polysulfomethyl A columns (200 × 4.6 mm, 5 µm, 1000 Å, PolyLC, Columbia, Maryland) at a flow rate of 0.95 ml/min using the Agilent 1100 HPLC previously described. The column compartment temperature was set at 35°C and sample injection volume was 1 ml. Separation solvents were solvent A (3% formic acid in water), solvent B (500 mM ammonium formate and 3% formic acid in water), and solvent C (acetonitrile). Initial conditions were 73% A: 2% B: 25% C, and then a linear gradient was performed to 75% B: 25% C in 20 min, with a stop time of 30 min. Samples were fractionated, dried, and reconstituted in 80 µl of 0.1% formic acid.

One minute fractions were collected starting at 3 min and continuing until 34.9 min. Samples were dried by vacuum centrifugation at 45°C and reconstituted in 90 µl of 0.1% formic acid. Fractions 1–4 and 5–8 were combined and cleaned up with Pierce C-18 spin columns (PN 89870) according to the manufacturer's instructions due to the possible presence of some detergents. Fractions 9–24 were analyzed by direct injection. All samples were filtered through 0.22 µm Agilent spin filters prior to analysis.

Orbitrap analysis. Separation of the peptides was performed on a Thermo Proxeon easy nano-LC (Thermo Fisher Scientific). The peptides were separated using an Acclaim pepmap 100 C18, 2 cm, 75 µm, 3 µm 100 Å (Thermo Fisher Scientific, PN 164705) trapping columns and an Acclaim pepmap 100 C18, 15 cm, 75 µm id, 3 -µm particle size 100 Å (PN ES800) analytical column. The sample was loaded with 80 µl of 0.1% formic acid in water. The injection volume was 10 µl. A gradient of 0.1% formic acid in water (pump A) and 0.1% formic acid in acetonitrile (pump B)

was used. The gradient profile was as follows initially 3% B, 45% B at 90 min, 95% B at 100 min, 95% B at 105 min, 1% B at 106 min, and the analysis stopped at 110 min.

Parent ion scans were done in the LTQ Orbitrap Velos (Thermo Fisher Scientific) using 60 000 resolution over the mass range of 400–1800 m/z. The top 10 peptides were selected for fragmentation by high collision dissociation (HCD). The HCD settings were minimum signal threshold 500, resolution of 7500, isolation width of 2 m/z, stepped collision energy at 40 and 50 V, default charge state of 2, and an activation time of 0.1 ms. Dynamic exclusion was done with a repeat count of 1 with a repeat duration of 20 s. An exclusion list of up to 50 precursors was created and the exclusion duration was 20 s. Exclusion was done relative to mass with a 2.5 AMU high limit and an 1.25 AMU low limits. Charge state screening was enabled and a charge state of 1 was rejected. The monoisotopic precursor selection was turned off because it was found that the presence of iTRAQ reagents interfered with the natural isotopic patterns of the peptides. Mass exclusion lists containing the precursors for high confidence peptides were created for fractions containing more than 100 identified peptides, and the fractions were repeated to improve coverage. Mass spectral data was processed using Thermo Proteome Discoverer 1.4. These peak lists were searched by Sequest against a rat database downloaded from NCBI with limits to Refseq. The database rat_4_10_15_fasta was searched using fixed modifications on cystine (metylthio) and any N-terminus or lysine (iTRAQ 8-plex) and variable modifications applied to methionine (oxidation), serine/tyrosine/threonine (phosphorylation), tyrosine (iTRAQ 8 plex), and asparginine and glutamine (deamidation). Proteome Discoverer processed the raw data with the following parameters: the mass tolerance values were set at 10 ppm for precursor ions and 0.8 Da for fragment ions, the enzyme was set to trypsin, the maximum number of modifications per peptide was 4, and the maximum number of missed cleavages was 2. Only scans with a 1% FDR as determined by percolator were used for protein identification.

Quantitative iTRAQ data analysis. Scaffold Q+ (version Scaffold 4.2.1, Proteome Software Inc, Portland, Oregon) was used to quantitate peptide and protein identifications from MS/MS spectra. Peptide identifications were accepted if the probability was $>$ 95.0% by the Scaffold Local FDR algorithm. Protein identifications $>$ 99.0% probability with at least 2 identified peptides and probabilities were assigned by the Protein Prophet algorithm (Nesvizhskii *et al.*, 2003). Proteins were grouped into clusters containing similar peptides not differentiable by MS/MS analysis alone to satisfy the principles of parsimony, correcting channels as described in i-Tracker (Shadforth *et al.*, 2005). Acquired intensities were globally normalized across all acquisition runs. Individual quantitative samples were normalized within each acquisition run. Intensities for each peptide identification were normalized within the assigned protein, and the reference channels were normalized to produce a 1:1 fold change. All normalization calculations were performed using medians to multiplicatively normalize data. A $\pm$ 1.3-fold threshold was used to identify differentially expressed proteins as described by Ahn *et al.* (2014).

Statistics: Bioplex data. Bioplex data were imported into GraphPad Prism (GraphPad Software, Inc; LaJolla, California) for analysis. A nonparametric Kruskal-Wallis ANOVA by ranks with *post hoc* Dunnett's multiple comparison test was used to determine statistical difference among dose groups. A 1 sample *t* test compared with a theoretical mean of 1.0-fold change was used to determine difference from control for each dose group. A P value $<$ .05 was considered statistically significant.

Gene panel selection. The gene panel was determined using 2 computational approaches: (1) a coexpression modules approach using iterative signature algorithms (Ihmels *et al.*, 2002) and (2) a pathway and network analysis approach (AbdulHameed *et al.*, 2014; Tawa *et al.*, 2014). The DrugMatrix liver gene expression data generated using Affymetrix GeneChip Rat Genome 230 2.0 Arrays were used for analysis. In the coexpression modules approach, genes were grouped into 78 distinct coexpression modules based on similarity of expression patterns across conditions, each condition defined as a particular compound-dose combination. The characteristic of correlated expression inherent in these modules implies that the module genes are associated with a common biochemical process. The resultant gene coexpression modules can be members of multiple modules. This is consistent with the fact that genes are, in general, associated with multiple biochemical pathways. Gene coexpression modules associated with liver fibrosis were identified as those exhibiting an average absolute activation value $>$ 1.5 times control when exposed to compound-dose combinations that caused fibrosis (Dalmas *et al.*, 2011). Center genes were identified from these modules as those with absolute activation closest to the module average. These center genes were chosen to be part of the multiplex panel (Tawa *et al.*, 2014).

In a pathway and network analysis approach, liver fibrosis-relevant genes were identified and mapped to pathways and high-confidence human PPI networks. The standard differential expression and coexpression analysis approach was carried out using rank product and hierarchical clustering, respectively, to identify liver fibrosis-relevant genes (Breitling *et al.*, 2004; Gentleman *et al.*, 2004). These genes were mapped to high-confidence human PPI networks (Yu *et al.*, 2009). Cytoscape tools such as KeyPathway Miner and Clusterviz were used to extract network modules (Alcaraz *et al.*, 2012). Network modules represent closely connected regions of the network and are expected to participate in similar function. Network modules with high activation scores in DrugMatrix liver fibrosis conditions and enrichment in known fibrosis-related genes were extracted. Differentially expressed genes in this module were chosen to be part of our multiplex panel (AbdulHameed *et al.*, 2014).

Bioplex assay. For the Bioplex assay, a custom QuantiGene 2.0 Plex assay was developed (Affymetrix) with 71 target genes plus 3 housekeeping genes. Using 150 ng RNA input, samples were processed following the manufacturer's instructions for purified RNA with use of the Hand-Held Magnetic Plate Washer. Plates were read immediately following the final wash using the BioPlex 200 instrument (BioRad, Hercules, California). The following parameters were set on the BioPlex instrument: sample size = 100 µl; DD Gate = 5000–25 000; Timeout = 45 sec; and Bead Event/Bead Region = 100.

Bioplex data analysis. For each sample, the average signal intensity was determined as recommended by the manufacturer. Duplicates were averaged. The average background signal for each gene was subtracted. Assay limit of detection was determined by adding 3 standard deviations of assay background signals to the average intensity of the background control wells. Probes with all intensities below the assay limit of detection

were removed from the final analysis. The test gene signal was divided by the average intensities of the 3 normalization genes (*Gapdh, Hprt1, Ppib*) as previously described (Vandesompele *et al.*, 2002). For each test gene, the fold change was calculated by dividing the normalized value for the treated samples by the normalized value of the vehicle-treated controls. Fold changes were plotted as $\log_2$ ratio. Gene expression data were imported into Partek Genomics Suite 6.0 (Partek, Inc, St Louis, Missouri). Principal component analysis and ANOVA were used for multivariate interpretation to determine sources of variation across sample groups (Joliffe and Morgan, 1992). Differentially expressed genes were determined by ANOVA with contrasts, setting the ANOVA factors as the microscopic endpoints of fibrosis or collagen accumulation (any score > 0). ANOVA variables were fibrosis score 0 (none) vs score of > 0 (minimal, mild, moderate, and marked). For hierarchical biclustering, differentially expressed genes were standardized by setting the genes expressed to a mean of zero and scaling to a standard deviation of 1. Euclidean geometry was used to cluster row and column dissimilarity using a method of average linkage.

Random forest classifier. Random forest analysis was used to identify the top genes that contribute most to the classifier performance. The microarray gene expression data were used as the training set, and the Bioplex data were used as the testing set. Only genes measured in both the Bioplex and the microarray data were used to build the classifier. Histopathology was used to categorize the animals as true positives or true negatives for the fibrosis phenotype (all classifications > 1).

PCOLCE ELISA assay. PCOLCE protein ELISA assays were performed on rat plasma according to the manufacturer's instructions (Cusabio, Wuhan, Hubei Province, China). Kruskal-Wallis ANOVA with *post hoc* Dunn's multiple comparison test was used to determine statistical significance.

Results

Histopathology

Two separate groups of experimental animals were used in the analysis: the training set (group 1, processed for microarray analysis) and the testing stet (group 2, processed for Bioplex analysis). In group 1, male Sprague Dawley rats were administered compounds by oral gavage for 5 days (Table 1). All chemicals except bromobenzene caused a dose-dependent increase in some or all of the clinical chemistries indicative of liver injury (AST, ALT, ALP, and LDH) (Table 2) The fibrogenic chemicals 4,4′-MDA (Figs. 1A–C) and allyl alcohol (Figs. 1D–F) caused a dose-dependent increase in fibrosis. The fibrosis pathology was comorbid with a dose-dependent increase in inflammation, bile duct hyperplasia, and hepatocellular necrosis Supplementary Table 1. Animals receiving the highest doses gained less weight over the 5-day exposure interval than their low-dose counterparts.

Carbon tetrachloride caused a dose-dependent increase in vacuolation confirmed to be lipid accumulation via Oil Red O histochemical reaction (Figs. 1G–I). Centrilobular collagenous accumulation was confirmed by Masson's Trichrome and was interpreted to be a prefibrotic observation.

Vacuolation, confirmed to be lipid accumulation by Oil Red O, increased with dose in both carbon tetrachloride-treated animals (Figs. 2A–C). The nonfibrogenic compound bromobenzene did not cause microscopic evidence of fibrosis at any dose but lipid accumulation increased with dose administered (Figs. 2D–F). The observed pathology is consistent with bromobenzene's toxicological classification as a potent inducer of hepatic steatosis, and vacuolation was confirmed to be lipid using the Oil Red O histochemical reaction (Thoolen *et al.*, 2010). The highest dose of bromobenzene resulted in body weight loss over the study interval.

All doses of dexamethasone resulted in lipemia (milky white plasma) and marked cytoplasmic alteration characteristic of glycogen accumulation, which was confirmed using the Periodic acid-Schiff staining method (Thoolen *et al.*, 2010) (Figs. 2G–I). Slight necrosis was evident in some of the livers.

Comorbid histopathologies are summarized for all treatments and all doses in Supplementary Table 1.

Transcriptomics

Global transcriptomics using microarray technology and targeted gene selection and analysis using Bioplex technology were conducted. For both analyses, the gene signatures were targeted for analysis (see selection parameters in the Materials and Methods section for gene selection). Briefly, gene selection was achieved by generating coexpression modules, then selecting centroid genes with greatest fold changes from control ($n = 25$ in each method). The genes most correlated with the fibrosis pathology in the DrugMatrix database were selected. For inclusivity, we also used a less selective filtering method and selected approximately 16 genes with the greatest fold change representing the fibrosis-specific modules. Unbiased biclustering of the microarray transcriptomics data demonstrated that chemicals causing the fibrosis pathology clustered together (Figure 3, dark, clustered near the bottom and light bars indicating fibrosis grade). Carbon tetrachloride caused collagen accumulation in the centrilobular region, a pathology associated with prefibrotic lesions. Gene profiles for the higher doses of carbon tetrachloride showed expression patterns partially resembling the fibrotic phenotype (Figure 3).

To determine whether the comorbid pathologies of fibrosis, necrosis, inflammation, and vacuolation caused complementary changes in expression profile for the fibrogenic genes, we generated principle components analysis plots of the pathologies (Figs. 4A–D). Most of the variation in the data could be explained by the comorbid pathologies except vacuolation. Interaction analysis was conducted to determine which genes were specific to the fibrosis phenotype as opposed to necrosis and/or inflammation. Contrast analysis identified 51 of the 67 genes in the predictive panel (Supplementary Table 1) associated with the fibrosis phenotype, of which 6 overlapped with the inflammation phenotype and 1 overlapped with necrosis (Figure 5A). Twenty-four were unique to the fibrosis phenotype (Figure 5B).

Multiplexed Fibrosis Gene Panel

To test the predictive power of these genes in multiplexed format, a second set of animals was orally administered selected doses of the test chemicals (group 2, test set of experimental animals). Chemical dose groups were downselected to conform to the 96-well assay format of the multiplexed panel of presumptive fibrosis genes (Bioplex). Three of the 4 dose groups were evaluated for the fibrogenic chemicals allyl alcohol and 4,4′-MDA. A single dose with group-matched vehicle controls for each of the remaining chemicals was selected. The high doses of carbon tetrachloride, dexamethasone, and bromobenzene were selected. The fibrosis, lipid accumulation, and glycogen accumulation pathologies were comparable to the first set of animals (Figure 6).

TABLE 2. Blood Clinical Chemistries After Oral Administration in Rats (Group 1 Experimental Animals)

	LDH			AST			ALT			ALP		
	Average	SD	P*	Average	SD	P*	Average	SD	P*	Average	SD	P*
Vehicle	345.8	108.2	> 0.05	102.2	11.8	**0.005**	69.8	15.9	**0.020**	341.0	108.8	**0.049**
Allyl alcohol 20.9 mg/kg	399.8	307.4		108.6	28.3		89.4	11.9		338.2	72.4	
Allyl alcohol 27.0 mg/kg	562.4	217.4		601.2	642.0		289.8	292.5		394.2	137.2	
Allyl alcohol 34.8 mg/kg	462.6	252.3		671.8	521.9		264.6	161.2		537.8	256.3	
Allyl alcohol 45.0 mg/kg	445.4	329.6		**1049.8***	887.9		447.2	**295.4***		**663.6***	139.6	
Vehicle	412.6	193.5	> 0.05	111.2	28.3	> 0.05	73.2	12.3	> 0.05	289.4	66.6	> 0.05
Bromobenzene 124 mg/kg	580.4	214.1		116.0	14.3		81.2	12.5		277.4	43.7	
Bromobenzene 229 mg/kg	633.4	251.6		149.4	42.6		75.2	2.9		354.4	60.8	
Bromobenzene 424 mg/kg	502.0	281.7		227.6	220.3		164.2	177.1		316.2	50.2	
Bromobenzene 785 mg/kg	510.4	148.7		158.6	48.4		84.8	37.2		289.6	38.5	
Vehicle	547.0	214.8	> 0.05	107.0	20.7	**0.015**	65.8	12.7	**0.019**	331.8	76.1	> 0.05
Carbon tetrachloride 20.0 mg/kg	472.8	85.6		113.4	12.5		73.8	15.1		350.4	33.1	
Carbon tetrachloride 43.1 mg/kg	693.8	230.7		144.4	51.3		70.0	8.5		406.0	69.6	
Carbon tetrachloride 92.8 mg/kg	594.6	236.5		143.4	40.3		94.0	46.2		369.0	110.5	
Carbon tetrachloride 200 mg/kg	505.6	35.6		**194.4***	25.9		**116.2***	33.5		490.6	156.2	
Vehicle	412.2	140.3	> 0.05	95.2	12.6	**0.001**	69.6	12.3	**0.002**	399.6	99.7	**0.012**
4,4′-MDA 22.0 mg/kg	451.6	147.7		113.4	12.9		68.4	7.7		338.8	82.7	
4,4′-MDA 59.7 mg/kg	554.6	34.3		**301.6***	67.2		**269.0***	157.2		499.8	95.3	
4,4′-MDA 162.0 mg/kg	402.2	83.0		**381.2***	91.1		**217.6***	31.5		**603.2***	124.7	
Dexamethasone, 1 mg/kg[a]	759.2	230.0	**0.032**	313.0	65.0	**0.008**	239.4	48.9	**0.008**	359.4	97.3	> 0.05

[a]Dexamethasone shares a vehicle control with 4,4′-MDA; 4,4′-MDA, 4,4′-MDA.

*P value, Kruskal Wallis ANOVA by Ranks with *post hoc* Dunn's comparison test,*(bold)$P < .05$ compared with control.

Isolated liver RNA was incubated with microbead-bound capture probes specific for the presumptive fibrogenic genes and 3 housekeeping normalization genes. All fluorescence intensity values for 4 genes (*Dram1*, *Myoc*, *Pdgf*, and *Lama5*) fell below the limits of assay detection. These genes were excluded from further analysis. For a complete list of differentially expressed genes, refer to supplemental data (Supplementary Table 1).

The expression patterns of the 67 genes measured by the Bioplex multiplexed assay correlated positively with the expression patterns reported in the DrugMatrix database ($R^2 = 0.79$; Figure 7A). The average log-ratio versus control across all samples showing fibrosis for genes on the Bioplex assay was well correlated with the microarray data in the original set of test animals ($R^2 = 0.86$; Figure 7B).

Differential gene expression was analyzed by hierarchical biclustering with the fibrogenic compounds (all dose groups) (Figure 8). Of the 67 genes available for analysis on the panel, fibrogenic compounds causing fibrosis clustered separately on the y-axis, with the exception of 2 allyl alcohol-treated animals. Dose groups with the fibrosis phenotype clustered separately from the lipid and glycogen accumulation phenotypes (Figure 8). Carbon tetrachloride (the delayed-onset fibrogenic chemical) showed a gene expression profile with features of both the nonfibrogenic and fibrogenic doses of the other compounds. Gene expression profiles for 2 allyl alcohol exposures with the fibrosis phenotype were more similar to the nonfibrogenic compound dose gene expression patterns than the fibrogenic chemicals. All other fibrogenic compound dose groups with the fibrosis phenotype clustered together. All of the fibrosis-positive animals dosed with 4,4′-MDA had comparable expression patterns (Figure 8).

Dose groups causing fibrosis produced more differential gene expression as compared with dose groups without fibrosis (Figure 9). The difference was most pronounced in upregulated genes (Figure 9). Twelve genes were downregulated in the animals exposed to nonfibrogenic compounds and upregulated in fibrogenic compound dose groups ($> \pm 1.5$-fold [average] represented by dashed lines in Figure 9 and listed in Table 3; *Col1a1*, *Col1a2*, *Col4a1*, *Cp*, *Cyba*, *Fbn1*, *Itgal*, *Itgb2*, procollagen C-endopeptidase enhancer *[Pcolce]*, urokinase plasminogen *[Plau]*, *Lamc2*, and *RT1-Da*). Of the 67 genes on the final panel, 16 were $< \pm 1.5$-fold-expression (Figure 9; Supplementary Table 1). Expression of 51 out of the 67 genes (76% of the panel) was ± 1.5-fold control expression for fibrogenic compounds with microscopic evidence of fibrosis (Supplementary Table 1). For most of the genes in the panel, expression of the carbon-tetrachloride dose group was midway between fibrosis-positive compound dose groups and nonfibrogenic compound dose groups (Figure 9, orange middle line). Nonfibrogenic compounds induced differential expression in 33 out of the 67 genes (50% of the panel). Gene expression was anticorrelated with fibrogenic, fibrosis-positive cohorts for 12 of these genes (Table 3), further supporting specificity of the expression pattern of these 12 genes for the fibrosis phenotype.

Classifier for Predicting Fibrosis Development

The gene panel tested in the group 1 experimental animals was used as the training data set to build a classifier for predicting fibrosis. Only genes present in both microarray and Bioplex data sets were used to build the classifier (59 of 62 genes). Of the 77 available samples, 19 were classified as true positives and 58 were classified as true negatives by histopathology. The internal cross-validation estimate of error rate was 2.6 for the training data set (Table 4). Random forest was used to identify the top genes that contribute most to the classifier performance (Table 4; Supplementary Figure 1). The random forest classifier was tested using the Bioplex data set. Of the 35 total animal exposures, 13 exposures produced fibrosis with a histopathology score > 2 (true positives) and 22 exposures produced no fibrosis by histopathology (true negatives). The accuracy of

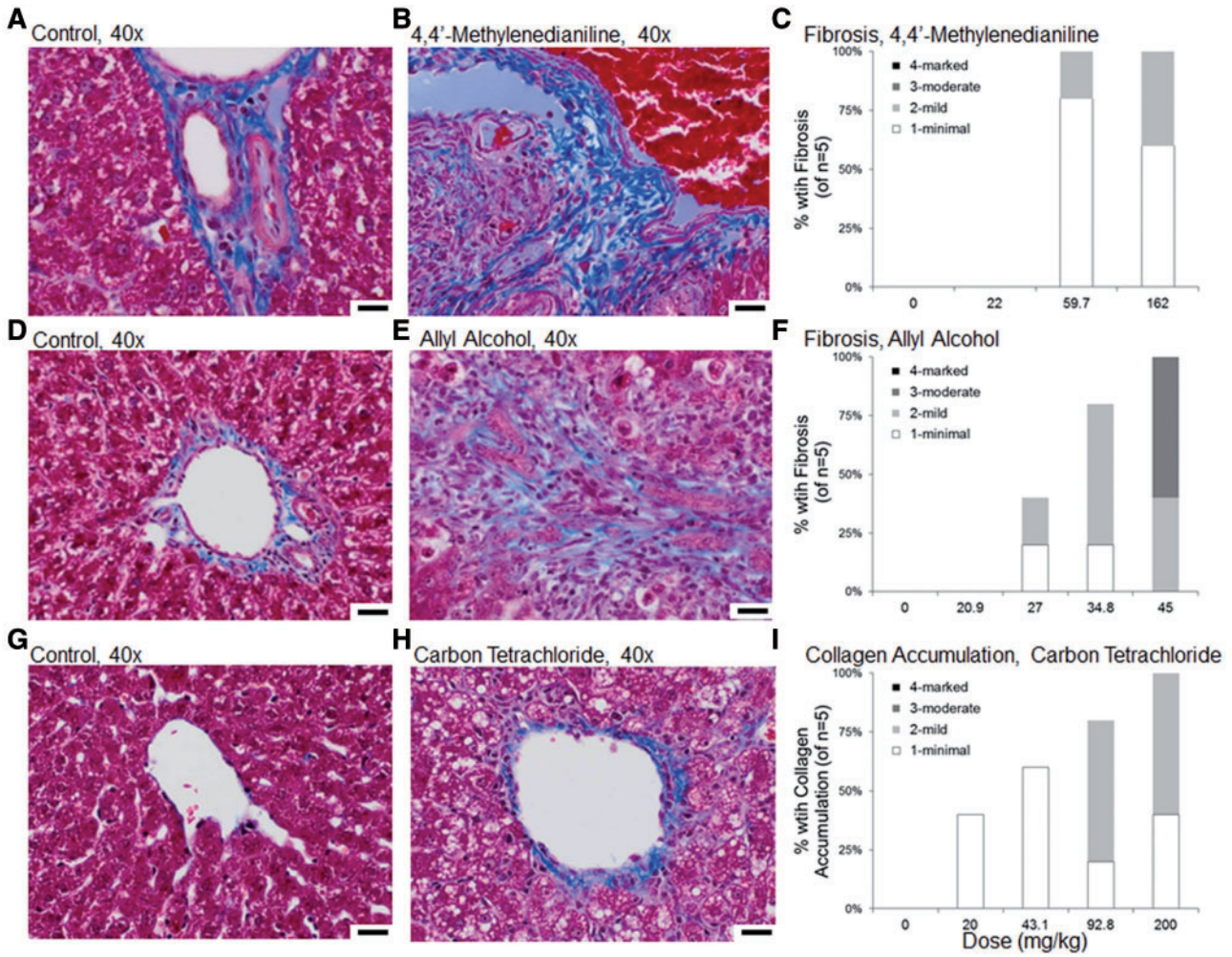

FIG. 1. Periportal fibrosis after 5-day oral administration of 162 mg/kg/day 4,4′-methylenedianiline (4,4′-MDA) and 45 mg/kg/day allyl alcohol, and prefibrogenic lesions in centrilobular region after 200 mg/kg/day carbon tetrachloride administration (group 1 experimental animals). A, Bile duct in control livers; region around bile duct denotes normal collagen. B, Periportal region, with increased collagen (fibrosis) and bile duct hyperplasia. ×40 magnification. C, Quantification from $n = 5$ animals per dose group for the fibrosis endpoint. Portal tract in livers from (D) control and (E) allyl alcohol-treated animals, quantified in (F) from $n = 5$ animals per dose group. G, Centrilobular vein in control animals. H, Centrilobular collageous accumulation demonstrated by halo rimming a centrilobular vein in carbon tetrachloride-treated animals, quantified in (I) from $n = 5$ animals. ×40 magnification; black scale bar, 20 μm. Masson's trichrome.

prediction was 88.6% (Table 4). Area under the receiver operator curve was 0.88 for the test set of data.

Protein Expression in the Plasma

Four of the genes included on the panel (*Lcn2*, α-2 macroglobulin [*A2m*], *Pcolce*, and *Lbp*) were part of a coexpression module including *A2m*, the gene encoding a protein used in the Fibrosure test for fibrosis or steatohepatitis (Rossi *et al.*, 2003). The differentially expressed genes showed an expression pattern unique to the fibrosis phenotype and fibrogenic chemical classification (Figs. 5 and 10A). *Pcolce* was the most differentially expressed gene in the fibrosis cohorts (Figs.5 and 10A). *Pcolce* expression levels induced by dexamethasone and bromobenzene were anticorrelated with corresponding gene expression levels induced by 4,4′-MDA and allyl alcohol (both fibrogenic compounds) (Figure 10A). The protein product of *Pcolce* was significantly and dose-dependently upregulated in plasma in animals dosed with fibrogenic chemicals relative to nonfibrogenic chemicals (Figure 10B).

Global semiquantitative proteomics analysis (iTRAQ analysis) identified protein products of a subset of the 24 genes differentially expressed in liver tissue specific for the fibrosis phenotype (Table 5; Figure 5B). Six protein products were identified in plasma, 4 in the serum, and 2 in the liver tissue (Table 5). All protein products were identified in the contrast analysis as specific for the fibrosis phenotype. The direction of the changes in protein products matched the transcriptomics data with the exception of insulin-like growth factor binding protein complex acid labile subunit precursor. This protein was decreased in expression in plasma but the genes *Igfbp1* and *Igfbp2* were upregulated in liver tissue.

Categorization of Fibrogenic Signature Gene Panel

Differentially expressed genes in the fibrogenic signature gene panel were categorized into the following mechanistic groups based on a review of the literature for each gene: hyperplasia, fibrosis and extracellular matrix (ECM) degradation, inflammatory signaling/chemotaxis, xenobiotic metabolism, and contractility (Figure 11). Twelve genes upregulated above control expression by at least 1.5-fold in the fibrosis-inducing compound-dose groups showed the opposite expression pattern in the nonfibrogenic compound-dose groups (group 2 Bioplex

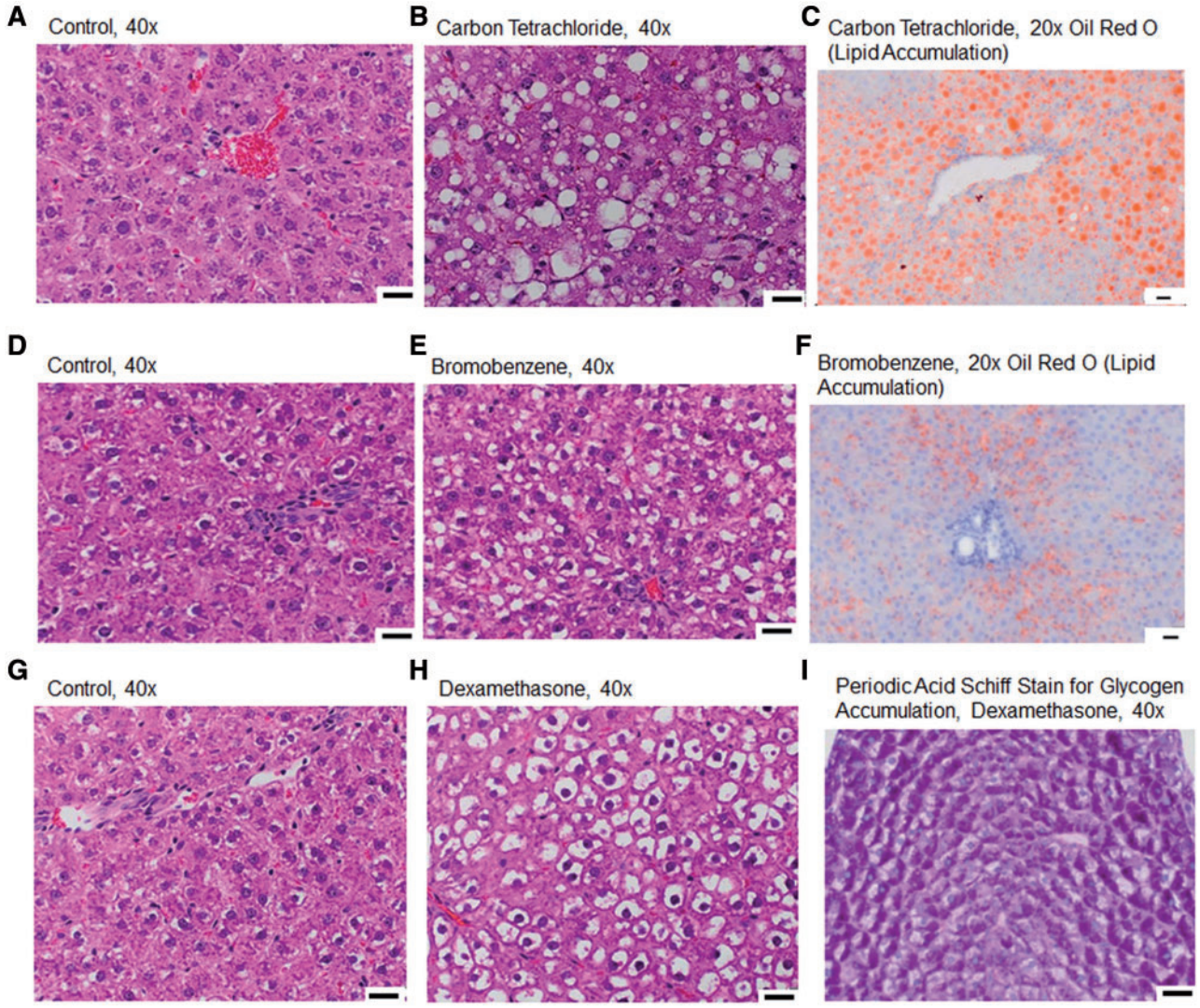

FIG. 2. Liver lipid accumulation after 5-day oral administration of 200 mg/kg/day carbon tetrachloride or 785 mg/kg/day bromobenzene, and glycogen accumulation after 1 mg/kg/day dexamethasone oral administration (group 1 experimental animals). A, Control livers, hematoxylin, and eosin staining. B, Increased vacuolation after carbon tetrachloride administration, ×40 magnification, (C) confirmed lipid accumulation with Oil Red O staining, ×20 magnification. D, Control livers, hematoxylin, and eosin staining. E, Increased vacuolation after bromobenzene administration, ×40 magnification, (F) confirmed lipid accumulation with Oil Red O staining, ×20 magnification. G, Control livers, hematoxylin, and eosin staining. H, Increased cytoplasmic alteration after dexamethasone administration, (I) confirmed to be glycogen accumulation by periodic acid-Schiff's staining. ×40 magnification. Black scale bar, 20 μm.

experimental animals; Table 3 and Figs. 9 and 11). These genes were associated with multiple mechanistic categories of fibrosis, including inflammation and chemotaxis, and ECM deposition/degradation (Figure 11). None of the anticorrelated genes were associated with hyperplasia or contractility (Figure 11; Table 3).

DISCUSSION

The observations in this study demonstrate (1) the predictive power of bioinformatics-based gene signatures for hepatic pathologies, (2) the utility of multiplexed technology in testing these predictions, and (3) novel plasma/serum-based biomarkers of fibrosis. Transcriptomics data (microarray or Bioplex) were 90%–95% correlated with the DrugMatrix repository predictions. Of the 67 signature genes evaluated in the Bioplex assay, 51 were consistent with predictions (76% accuracy). This study provides experimental verification of the computational and bioinformatics methods used to generate the gene signatures (AbdulHameed *et al.*, 2014; Tawa *et al.*, 2014). This research demonstrates the utility of a multiplexing strategy to evaluate biomolecular signatures linked to microscopic indicators and could suggest a novel panel of biomarkers for earlier predictive assays to complement existing clinical diagnosis using biopsied tissue (Alfirevic and Pirmohamed, 2012; Cui and Paules, 2010; Fontana, 2014; Meldrum *et al.*, 2011; Zhang *et al.*, 2014). Interpreting gene module activation in the context of "Adverse Outcomes Pathways" could provide a more sensitive and specific way to guide regulatory decisions when evaluating risks associated with similar and/or novel drugs and industrial toxicants (Vinken, 2013).

Bioinformatics-Based Database Mining of Public Data Repositories

The main purpose of this study was to test the fidelity of the gene panel developed by mining large public repositories of microarray transcript expression data (more than 3200 exposures) linked to liver histopathology in rodents (Ganter *et al.*, 2005; National Toxicology Program, 2010). Testing the

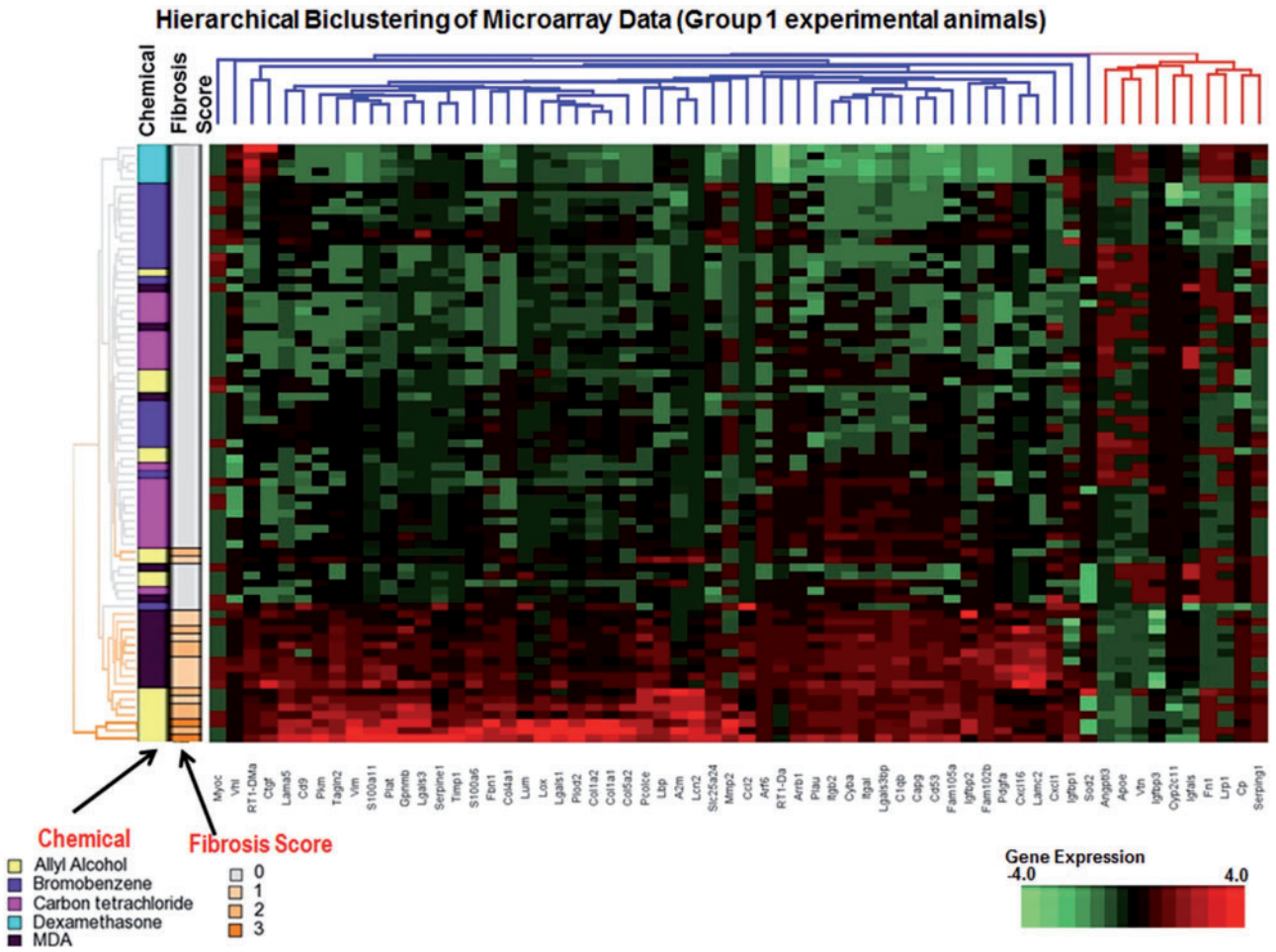

FIG. 3. Hierarchical biclustering of fold-changes in gene expression patterns for 62 genes on the microarray in fibrogenic and nonfibrogenic chemicals (group 1 experimental animals). Fold-changes were determined for presumptive fibrosis gene indicators by microarray analysis and visualized by hierarchical biclustering. 4,4′-MDA, 4,4′-MDA; 0-no observable pathology; 2-mild pathology (> 30%–60% of tissue affected); 3-moderate pathology (> 60%–80% of tissue affected). Data were standardized; red indicates higher expression relative to mean, and green indicates lower expression relative to mean. Full color version available online.

phenotypic response using multiplexed gene expression assays independent of the microarray platform demonstrated the fidelity of the gene panel, supporting specificity for the observed fibrosis pathology. The delayed-onset fibrogenic agent carbon tetrachloride demonstrated a gene expression pattern intermediate to the fibrotic phenotypes in the biclustering analysis, indicating an association between level of gene expression and time to fibrosis onset that is supported by the literature (National Toxicology Program, 2011).

Our biomarker selection algorithms combine phenotypic- and mechanism-based gene candidates. Relying solely on mechanism-based markers is complicated by the fact that most cases of drug-induced hepatotoxicity are idiosyncratic, and only 30% of instances correlate with cause in the national registry (Alfirevic and Pirmohamed, 2012). Further, phenotypic linking of gene expression signatures could identify novel molecular mechanisms linked to drug-induced toxicity and improve the fidelity of biomarker-based diagnostic assays (Cui *et al.*, 2013).

The heterogeneity in individual responses of specific genes underscores the need for multigene assays to screen multiple targets (Meldrum *et al.*, 2011). Personalized medicine hinges on using host-specific genome data or tissue-specific gene expression profiling to improve diagnosis and minimize the effect of interindividual variability (Fontana, 2014). One of the clinically used noninvasive diagnostic tests for liver injury is the FibroSure panel, which is based on a predictive algorithm incorporating age, gender, and blood concentrations of the analytes α2-macroglobulin, haptoglobulin, bilirubin, and apolipoprotein A1. Although the panel correlates well with late-stage fibrosis diagnosed by liver biopsy, it lacks sensitivity and specificity as an early (stage 1–2) diagnostic indicator (Rossi *et al.*, 2003).

The high concordance of the gene signature panels with the predictions also supports the application of the bioinformatics approach to human repositories. The drug-induced liver injury network is currently collecting phenotypic data in conjunction with a repository of genomic DNA, serum, urine, and liver biopsies to develop personalized medicine approaches to treat drug-induced liver injury (Alfirevic and Pirmohamed, 2012). Testing the human homologues of our signature panel of genes for correlation with fibrogenesis may facilitate better characterization of biopsy specimens. Testing secreted proteins in plasma may facilitate earlier detection of fibrosis in susceptible individuals (Leung *et al.*, 2012).

Mechanisms of Hepatotoxic Injury for Toxicants

The mechanisms of hepatotoxicity of all toxicants used in this study were deliberately selected to represent fibrinogenic and nonfibrinogenic chemical-dose groups with different times to

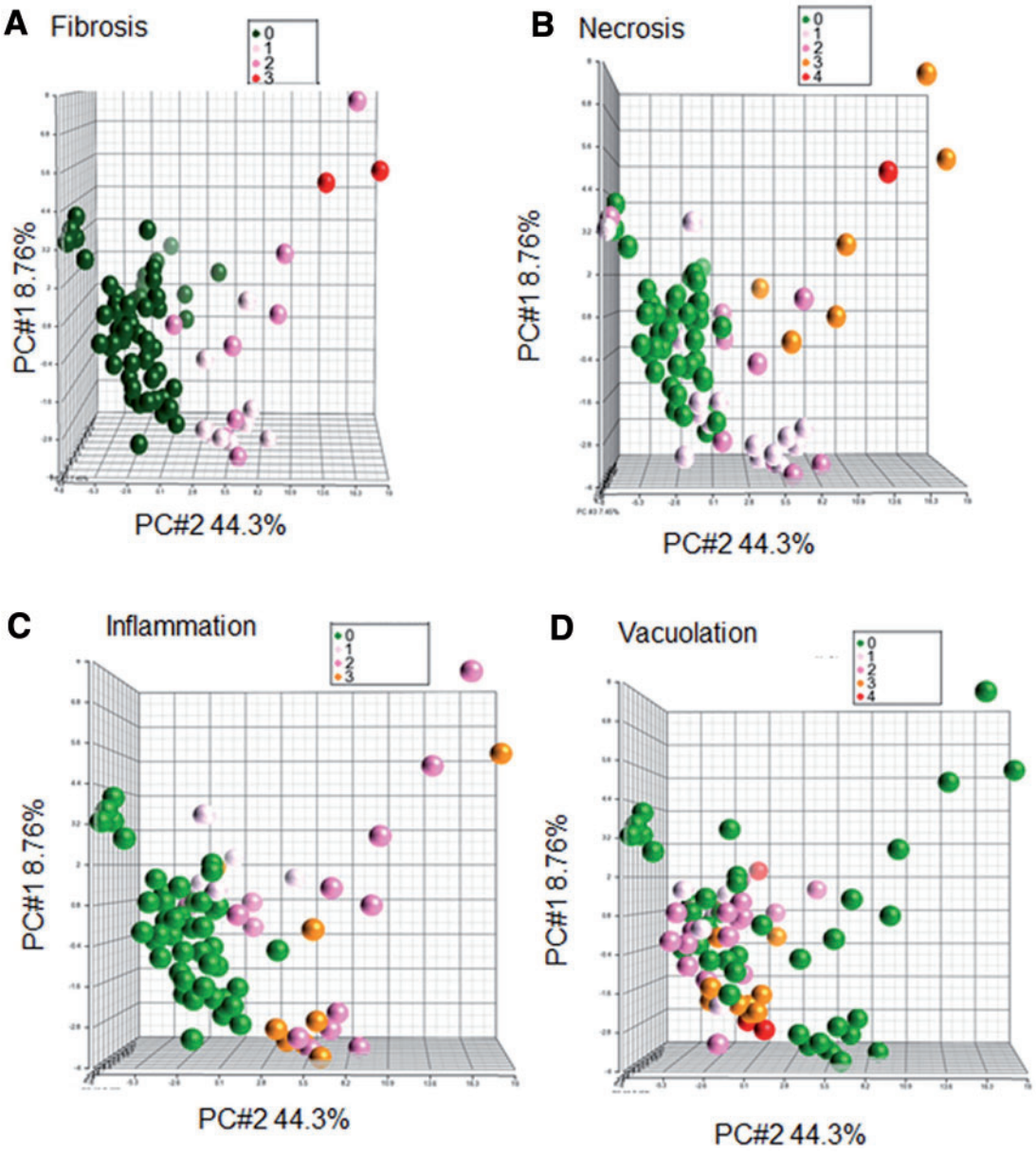

FIG. 4. Principal component analysis and inference analysis for 62 presumptive fibrogenic genes by microarray analysis (group 1 experimental animals). Comorbid pathologies of fibrosis (A), necrosis (B), inflammation (C), and vacuolation/lipid accumulation (D) were analyzed by principle components analysis. E, Biclustering analysis indicating cluster of genes by histopathology for the comorbid pathologies. 4,4′-MDA, 4,4′-MDA; 0-no observable pathology; 1-minimal pathology (> 0%– < 30% of the tissue affected); 2-mild pathology (> 30%–60% of tissue affected); 3-moderate pathology (> 60%–80% of tissue affected). Data were standardized; red indicates higher expression relative to mean, and green indicates lower expression relative to mean. Full color version available online.

injury onset (5 days to 2 weeks) (Yu *et al.*, 2002). In concordance with previous reports, allyl alcohol and 4,4′-MDA showed microscopic evidence of fibrosis within the 5-day study interval (Ganter *et al.*, 2005; National Toxicology Program, 2010). Allyl alcohol rapidly converts to acrolein in the periportal hepatocytes, resulting in rapid glutathione depletion and localization of fibrosis to the periportal region (Jaeschke *et al.*, 1987; Moustafa, 2001). Previous reports concur with our data demonstrating that *Tgfb1* mRNA expression increases with extent of fibrotic injury, with considerable interindividual variability (Jung *et al.*, 2000). Like allyl alcohol, 4,4′-MDA undergoes toxic metabolic conversion in the liver with localization of fibrotic injury to the periportal region (Zhang *et al.*, 2006). Genetic variation in the N-acetyltransferase family of hepatic enzymes correlates with extent of portal damage: the Sprague Dawley strain used in our study (fast acetylators) have correspondingly greater evidence of necrotizing hepatitis than Fisher 344 strains (slow acetylators) (Zhang *et al.*, 2006). Both allyl alcohol and 4,4′-MDA cause fibrosis by directly influencing myofibroblast proliferation. Myofibroblasts secrete cytokines and other catalysts of ECM formation. Thus, both chemicals caused fibrosis within a week of repeated dosing. In contrast, carbon tetrachloride fibrotic injury requires more than 2-4 weeks of repeated dosing (Ganter *et al.*, 2005; Weber *et al.*, 2003; National Toxicology Program, 2010). Carbon tetrachloride directly causes structural damage to zone 3 hepatocytes by cytochrome P450-dependent conversion to the free radical $\bullet CCl_3$. Sustained tissue necrosis by free radical damage overwhelms repair mechanisms, leading to

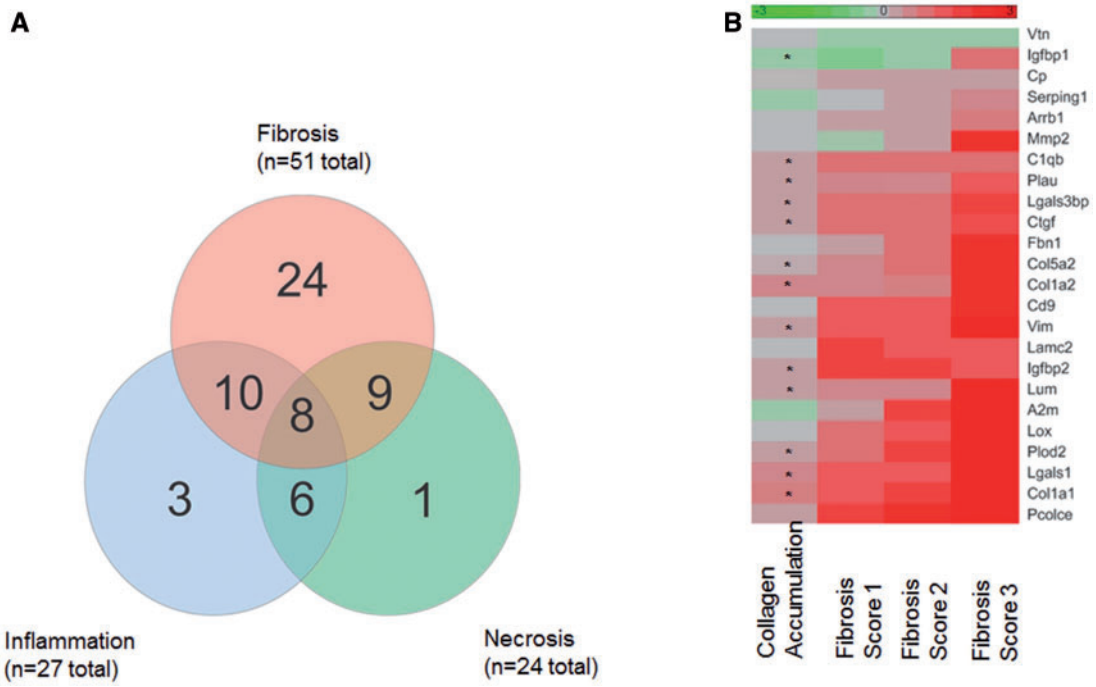

FIG. 5. Genes associated with fibrosis, inflammation, and necrosis endpoints (group 1 experimental animals). A, Venn diagram indicating genes unique to fibrosis endpoint, inflammation, or necrosis. B, 24 genes unique to the fibrosis endpoint alone identified by interference analysis (FDR < 0.05 for necrosis, fibrosis, inflammation; ANOVA with contrasts); *, potential early indicators of fibrotic injury; genes differentially regulated in early fibrosis.

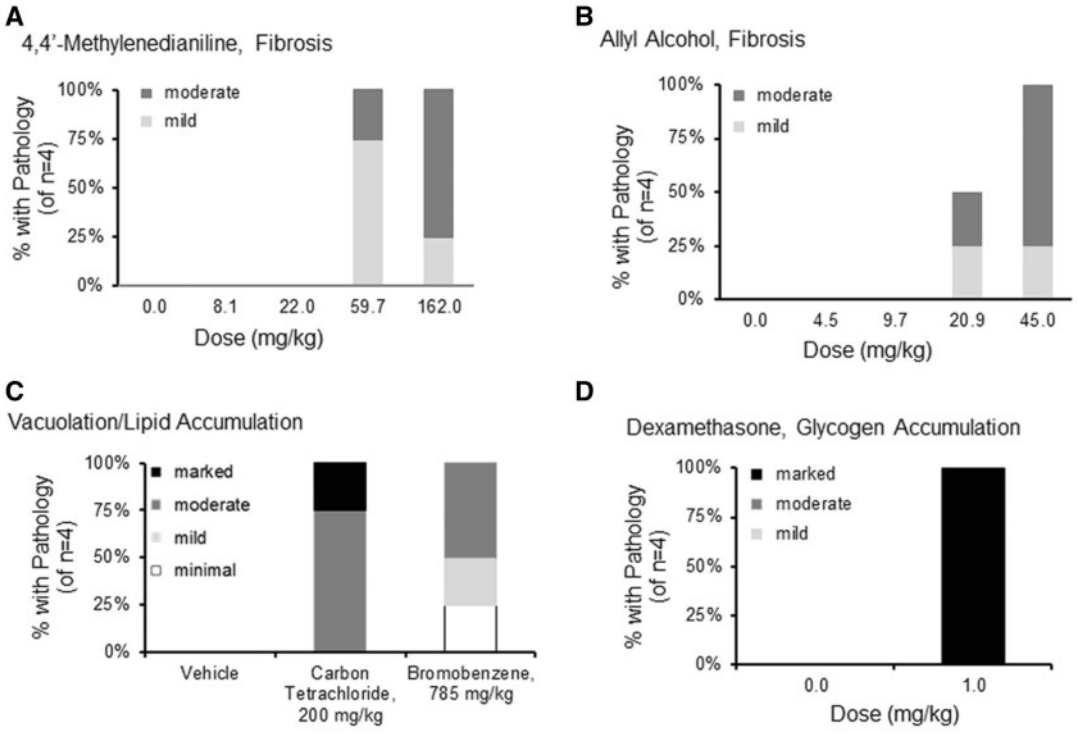

FIG. 6. Periportal fibrosis after 5-day oral administration of 4,4′-MDA or allyl alcohol, liver lipid accumulation after carbon tetrachloride and bromobenzene, and liver glycogen accumulation after dexamethasone in second "test" set of animals (group 2 experimental animals). A, Dose-dependent increase in fibrosis phenotype after 5-days oral administration of 4,4′-MDA and (B) allyl alcohol. C, Elevation of vacuolation indicative of lipid accumulation after 200 mg/kg carbon tetrachloride and 785 mg/kg bromobenzene treatment. D, Increased cytoplasmic alteration indicative of glycogen accumulation after 1 mg/kg dexamethasone administration.

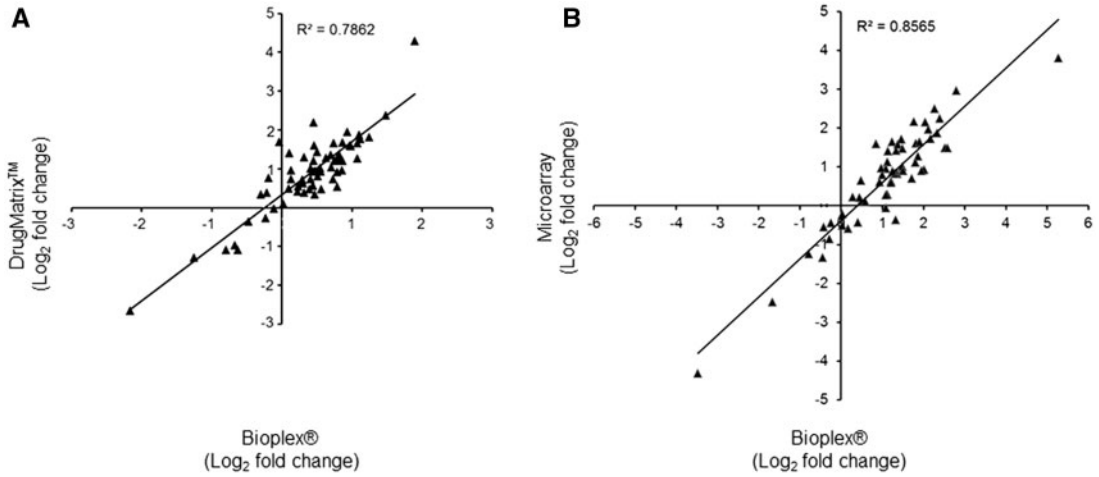

FIG. 7. Positive correlation between liver $\log_2$ fold-changes in gene expression from DrugMatrix, Bioplex (group 2 animals), and microarray data (group 1 animals). A comparison of $\log_2$ fold-changes of panel genes using data from the Bioplex multiplexed experiments (group 2 experimental animals) with (A) DrugMatrix database and (B) microarray $\log_2$ fold-changes in gene expression associated with fibrogenic chemicals that show histopathological evidence of periportal or subcapsular fibrosis (group 1 experimental animals). Allyl alcohol, 4,4′-MDA, 1-naphthyl isothiocyanate, crotamiton, testosterone, carvedilol, carmustine, vinblastine, beta-estradiol, and bezafibrate (5–7 days oral administration or intraperitoneal injection) at various doses scored fibrosis-positive in the DrugMatrix study. Allyl alcohol and 4,4′-MDA at high doses scored positive for fibrosis in this study on both microarray and Bioplex panels.

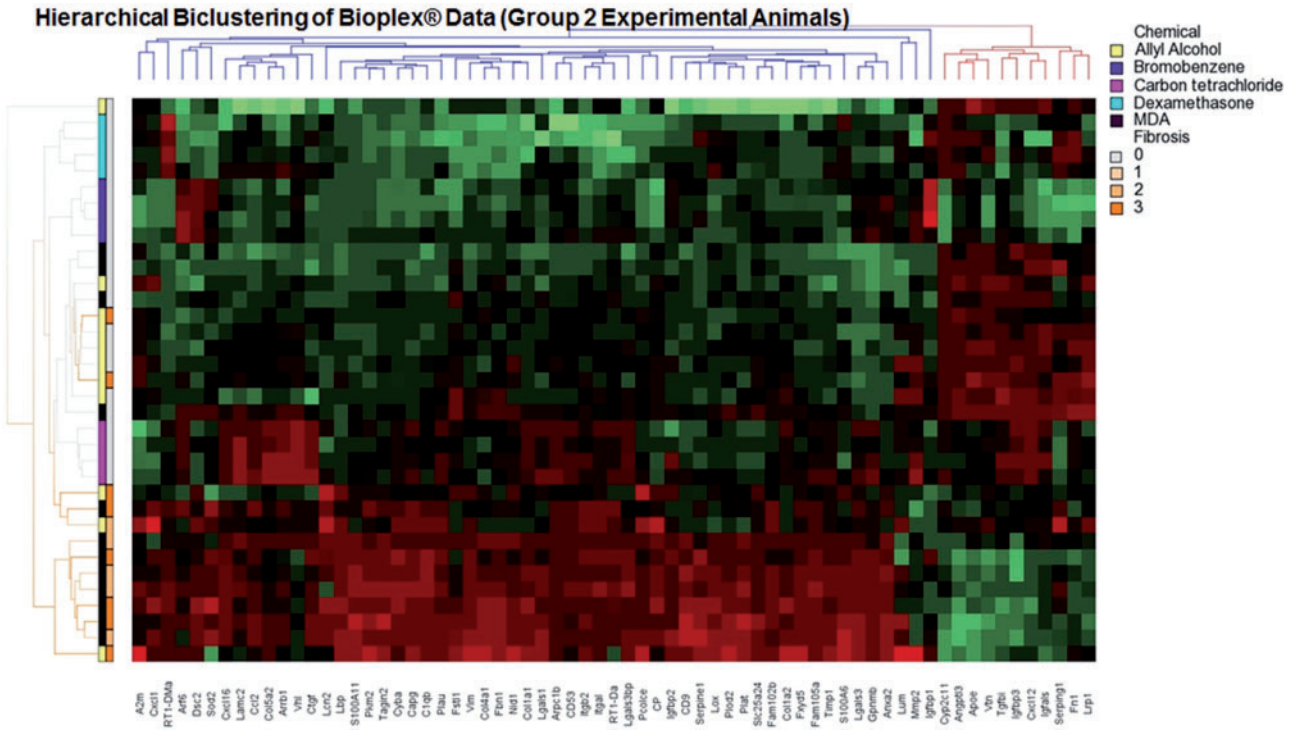

FIG. 8. Hierarchical biclustering of $\log_2$ fold-changes in gene expression patterns for 67 genes on the fibrosis gene panel in nonprefibrogenic and prefibrogenic pathologies (group 2 experimental animals). Log_2 fold-changes were determined for presumptive fibrosis gene indicators by multiplexed spectrophotometric Bioplex assay and visualized by hierarchical biclustering. 4,4′-MDA, 4,4′-MDA; 0-no observable pathology; 2-mild pathology (> 30%–60% of tissue affected); 3-moderate pathology (> 60%–80% of tissue affected). Data were standardized; red indicates higher expression relative to mean, and green indicates lower expression relative to mean. The genes listed are in the same order as Supplementary Table 1. Full color version available online.

a delay in the fibrosis phenotype (Friedman, 2008; Zhou *et al.*, 2013). The delayed time-to-onset of carbon tetrachloride-induced fibrosis allowed us to examine early markers of fibrosis, as evidenced by clustering of carbon tetrachloride-administered animals midway between the fibrogenic and nonfibrogenic compound-dose groups in Figure 8. Interaction between $\bullet CCl_3$ free radicals and cellular constituents directly impairs lipid metabolism shortly after initial dosing, leading to the early-onset fatty accumulation observed in our study (Weber *et al.*, 2003). Similarly, bromobenzene is an early onset inducer of lipid accumulation by conversion to its reactive metabolite (2,3- and 3,4-oxide derivatives). Like $\bullet CCl_3$, bromobenzene reactive intermediates also impair mitochondrial fatty acid β-oxidation to cause fatty accumulation (Lertratanangkoon *et al.*, 1993).

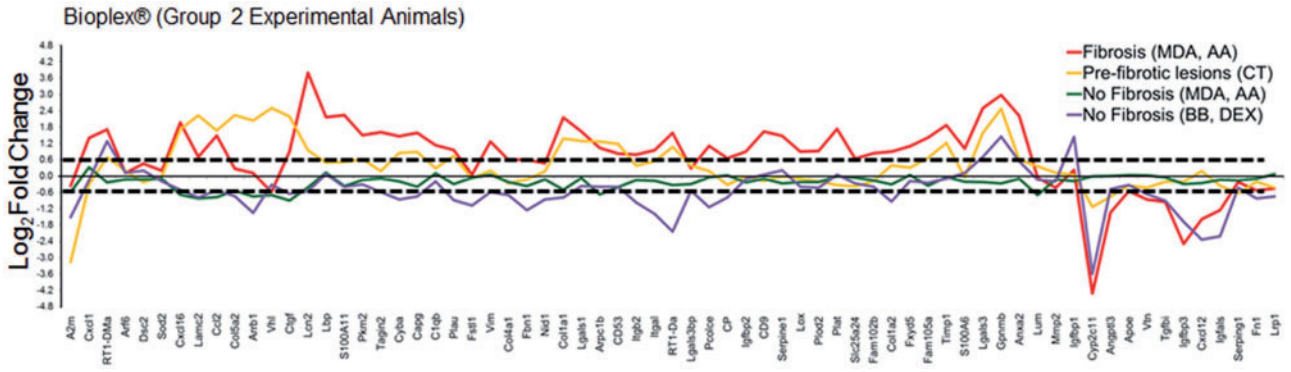

FIG. 9. Differentiable gene signature pattern for fibrogenic compounds with histopathological evidence of fibrosis in Bioplex data (group 2 experimental animals). Expression (log_2 or fold-change over vehicle control) for 67 signature fibrogenic genes were plotted in order of the biclustering analysis (Figure 7 and Supplementary Table 1). High-dose 4,4′-MDA and allyl alcohol (AA) exposures were associated with fibrosis. Carbon tetrachloride (CT) caused prefibrotic lesions. Low-dose 4,4′-MDA and allyl alcohol were fibrogenic chemicals without fibrosis. Bromobenzene and dexamethasone exposures correlated with histopathological evidence of vacuolation and/or glyocgen accumulation, without fibrosis. Dashed lines represent the 1.5-fold threshold for significance.

TABLE 3. Anticorrelated Signature Genes[a]

Gene	Fibrogenic Mechanistic Category
Col1a1	Fibrosis and ECM deposition/degradation
Col1a2	Fibrosis and ECM deposition/degradation
Col4a1	Fibrosis and ECM deposition/degradation
Cp	Inflammation/chemotaxis
Cyba	Xenobiotic metabolism
Fbn1	Inflammation/chemotaxis
Itgal	Inflammation/chemotaxis
Itgb2	Inflammation/chemotaxis
Lamc2	Inflammation/chemotaxis
RT1-Da	Inflammation/chemotaxis
Pcolce	Fibrosis and ECM deposition/degradation
Plau	Fibrosis and ECM deposition/degradation

[a]downregulated in response to nonfibrogenic chemicals and upregulated in response to fibrogenic chemicals producing fibrogenic phenotype; ECM, extracellular matrix.

TABLE 4. Random Forest Classifier Model Predictions: Training (Group 1) and Testing (Group 2) Sets of Experimental Animals and Data

	Sensitivity	Specificity	Accuracy	Kappa
Training (Microarray)[a]	94.7	98.3	97.4	0.93
Testing (Bioplex)	69.2	100.0	88.6	0.74

[a]internal cross-validation (estimate of error rate): 2.6.

Prolonged administration of the corticosteroid dexamethasone also inhibits fatty acid β-oxidation but overt fatty accumulation takes longer to manifest as compared with induction by either bromobenzene or carbon tetrachloride. Unlike these direct toxicants, dexamethasone induces steatosis secondary to a generalized suppression of the adrenal-hypothalamic-pituitary axis and demobilization of fat stores (Coiro and Goodman, 1987). However, the liver glycogen accumulation observed in our study is likely an early indicator of impending steatosis (Jackson *et al.*, 2008; Lupp *et al.*, 1998).

In the initial stages of fibrogenesis, the injury is reversible as cellular mechanisms promote apoptosis of fibrotic cells and tissue regeneration (Friedman, 2008). Thus, a concomitant increase in expression of both pro- and antifibrogenic genes would be expected as the system attempts to reestablish homeostasis. During the 5-day interval of our study, increases in pro- and antifibrogenic gene expression were observed after high dose allyl alcohol and 4,4′-MDA exposure (Figure 11). These findings are corroborated by fibrogenic mechanisms reported in the literature. For some genes, however, our study was the first to show change in expression in the early stages of the fibrogenic phenotype (eg, *Pcolce*). PCOLCE, the secreted protein product, was upregulated in the plasma in our study.

The liver has a high regenerative capacity after initial insult but long-term toxicant exposure overwhelms remodeling and repair mechanisms (Friedman, 2008). The adaptive immune response initiated in hepatic Kupffer cells and natural killer cells exacerbates the initial injury by releasing and recruiting proinflammatory mediators to the site of injury (Zhou *et al.*, 2013). Concomitant activation of hepatic stellate cells and proliferation of myofibroblasts produces ECM components resulting in fibrosis (Friedman, 2008). Genes in the signature panel directly or indirectly correspond with either the fibrosis phenotype or a pathology characteristic of irreversible, late-stage disease progression in postnecrotic and/or fibrotic injury (ie, hepatocellular carcinoma, cirrhosis).

Gene Signatures in Hepatotoxic Injury

Liver fibrosis is generally associated with chronic, low-dose toxicant exposure scenarios, but high doses of potent fibrogenic drugs and compounds can also cause fibrosis within 1 week (Ganter *et al.*, 2005; Hannivoort *et al.*, 2012; National Toxicology Program, 2010). The risk for irreversible damage and hepatic failure increases with percentage of affected tissue (Bataller and Brenner, 2005; Brenner, 2009). Early diagnosis and assessment of fibrotic damage can serve as an early predictor of liver injury after toxic insult (Baranova *et al.*, 2011). The genes in the signature gene panel for fibrosis can be mechanistically subdivided into 3 broad categories: hyperplasia and cell growth, fibrosis/decreased ECM degradation, and inflammatory signaling/chemotaxis (Figure 11) (Friedman, 2008). The observed differential expression patterns after fibrotic injury were mostly consistent with the current literature predictions. Some of the differentially expressed genes were previously associated with more advanced fibrotic injury, suggesting that our study is among the first to report these genes as acute to subacute injury indicators of fibrogenesis.

Growth factors and hyperplasia. The comorbidity of bile duct hyperplasia and fibrosis observed in our study has also been reported in

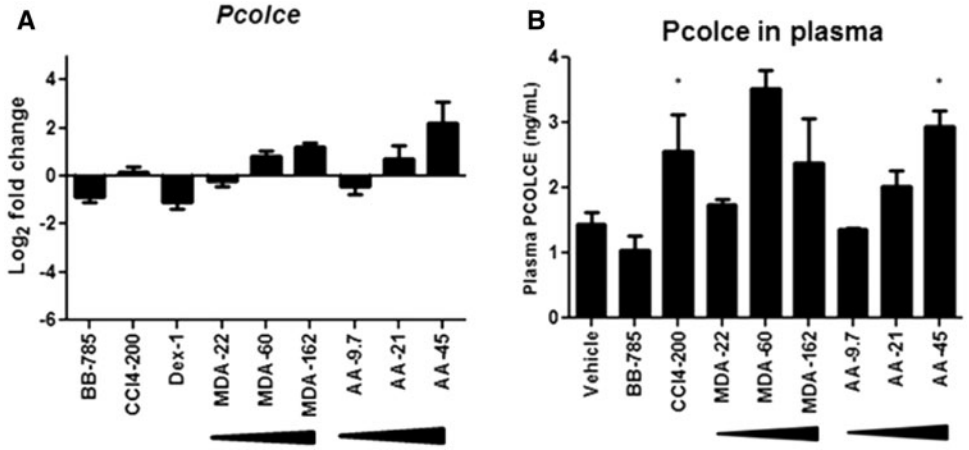

FIG. 10. Dose-dependent increase in expression of *Pcolce* in liver tissue and its protein product PCOLCE in plasma. Gene expression of *Pcolce* (A) and its protein product PCOLCE (B) was plotted in exposure groups segregated by chemical. Bromobenzene exposures correlated with histopathological evidence of vacuolation and/or necrosis. High-dose 4,4′-MDA and allyl alcohol exposures were associated with fibrosis histopathology without evidence of vacuolation. CT-induced prefibrotic lesions. MDA, 4,4′-MDA; AA, allyl alcohol, BB, bromobenzene, CCl4, carbon tetrachloride (doses in mg/kg); $P < .05$.

TABLE 5. Fold Changes in Tissue, Plasma, or Serum Protein Abundance Measured by iTRAQ Mass Spectrometry (Group 2)

	Protein[a]	GenInfo Identifier No	P*	Fold change[b]
Plasma				
	fibronectin precursor	186972114	< 0.0001	−1.3
	ceruloplasmin isoform 1 precursor	401461786	< 0.0001	2.5
	vitronectin precursor	162287178	< 0.0001	−1.6
	insulin-like growth factor-binding protein complex acid labile subunit precursor	71896592	< 0.0001	−1.4
	alpha-2-macroglobulin precursor	158138551	0.0370	2.2
Serum				
	vitronectin precursor	162287178	1.0000	−1.1
	ceruloplasmin isoform 1 precursor	401461786	< 0.0001	2.4
	alpha-2-macroglobulin precursor	158138551	< 0.0001	2.4
	complement C1q subcomponent subunit B precursor	9506433	0.5700	1.6
Tissue				
	fibronectin precursor	186972114	< 0.0001	1.4
	ceruloplasmin isoform 1 precursor	401461786	< 0.0001	3.0

[a]*Rattus norvegicus*.
[b]*fold change* (4,4′-MDA/vehicle).
*P value, Kruskal Wallis ANOVA by Ranks.

rodent models of chronic bile duct obstruction by bile duct ligation (Alpini *et al.*, 1988; Davis *et al.*, 1978; Despa *et al.*, 2005; Floyd *et al.*, 2010; Lahaye *et al.*, 1998; Zhao *et al.*, 2008). The proliferated cells are functionally complementary to ductular cells and regulate bile duct flow by hepatocyte Na/K-ATPase. The Na/K-ATPase is negatively regulated by FXYD-domain proteins under conditions of cirrhosis and bile duct hyperplasia (Figure 11) (Alpini *et al.*, 1988; Davis *et al.*, 1978; Despa *et al.*, 2005; Floyd *et al.*, 2010; Lahaye *et al.*, 1998; Zhao *et al.*, 2008). Differential expression of the insulin-like growth factor binding proteins (Figure 11) is consistent with recent reports showing differential expression among *Igfbp*-1, -2, and -3 (Chen *et al.*, 2006; Ghosh and Vaughan, 2012; Novosyadlyy *et al.*, 2005; Ross *et al.*, 1996). Protein products of *Igfbp* precursor were differentially expressed in the plasma in our study.

Fibrosis and ECM production/degradation. Hepatic stellate cells are activated in the early stages of fibrosis, initiating ECM production and collagen deposition characteristic of fibrotic injury (Brenner, 2009). *Tgfb1* encodes a multifunctional peptide which regulates proliferation, differentiation, adhesion, migration, and many other physiological and pathological functions (Causey *et al.*, 2012; Massague and Gomis, 2006). In the liver, *Tgfb1* encodes a master regulator of ECM production and hepatic stellate cell activation after toxic chemical injury (Ghosh and Vaughan, 2012; Liu, 2008; Liu *et al.*, 2010; Liu and Gaston Pravia, 2010; Van Wettere *et al.*, 2013). In contrast, the inducible form of TGF-β (*Tgfbi*) was downregulated in the livers with microscopic evidence of fibrosis in this study (Figure 11; Supplementary Table 1). This finding contrasts with recent studies in rodent models of chronic cholangitis and cirrhosis (Lu *et al.*, 2014; Nakken *et al.*, 2007). The reason for the discrepancy is unclear, although *Tgfbi*$^{-/-}$ mice have a heightened adaptive immune response (Hei *et al.*, 2011). An anti-inflammatory role for *Tgfbi* is concordant with our report of lower *Tgfbi* expression in animals with increased inflammatory infiltrate. In a recent study, apoptosis of hepatocytes correlated with high producers of TGF-β1, leading to fewer TGF-β1-expressing cells over time (Ueberham *et al.*, 2003). No compensatory proliferation of hepatocytes was

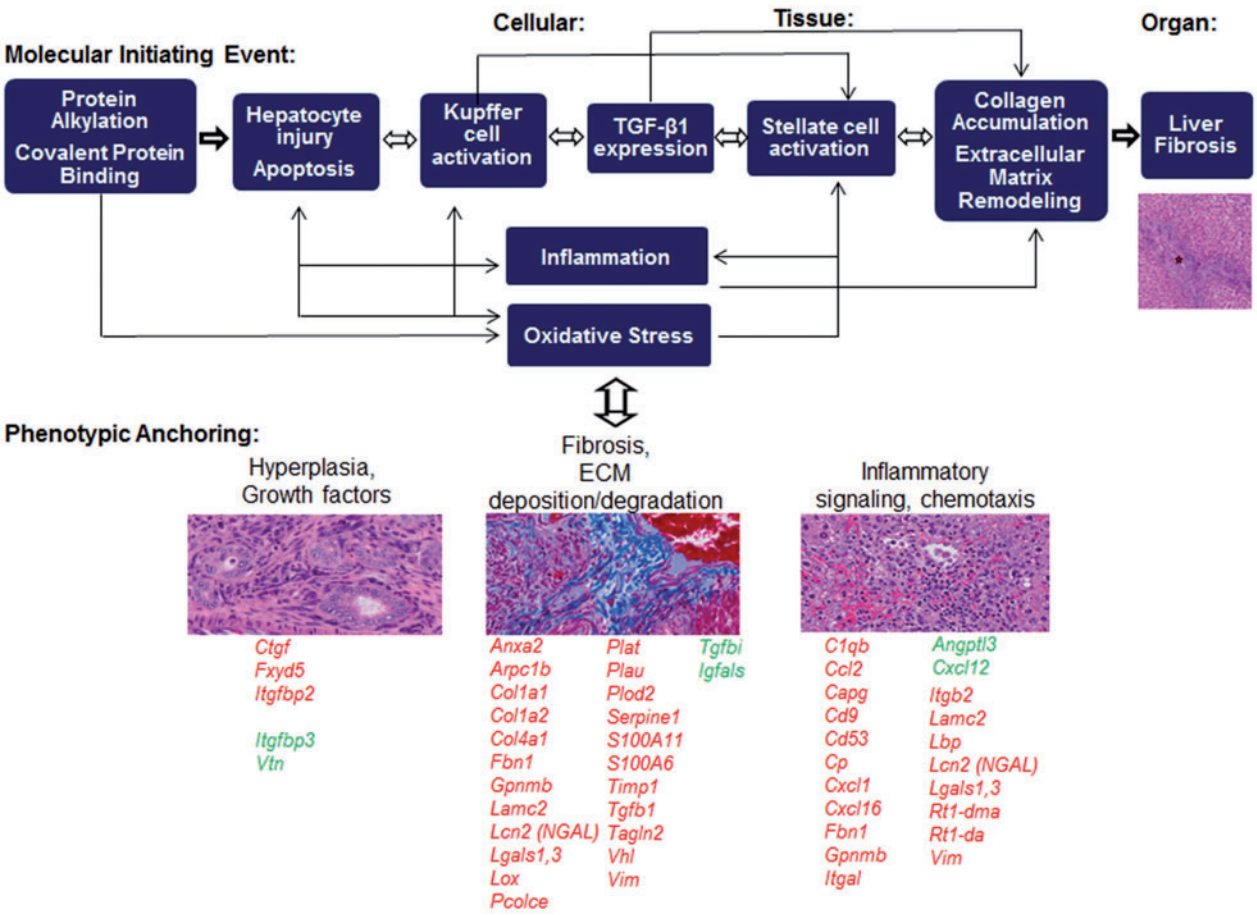

FIG. 11. Summary of differentially expressed genes by putative classification in the fibrogenic gene signature panels in the context of the current fibrosis adverse outcome pathway (Vinken, 2013). Red, upregulated > ×1.5; green, downregulated > 1.5-fold (Bioplex data); ECM, extracellular matrix; *results reported in the literature at later stages in disease progression with overt fibrosis and/or cirrhosis phenotypes. Full color version available online

detected. A similar phenomenon could be occurring in our study.

The protein encoded by *Tgfb1* stimulates expression of plasminogen activator inhibitor, a negative regulator of tissue-plasminogen activator (encoded by tissue plasminogen *[Plat]*) and urokinase plasminogen activator (encoded by *Plau*) (Figure 11). Plasminogen orchestrates degradation of ECM components. In the early stages of fibrosis, ECM degradation counterbalances production to repair hepatic injury, possibly accounting a compensatory upregulation of promoters and inhibitors of ECM production.

Upregulation of both positive and negative regulators of ECM deposition and degradation suggests an increase in tissue remodeling consistent with the early stages of fibrogenesis, when repair and return to homeostasis are counterbalanced with irreversible tissue scarring. The 5-day exposure interval in this study and the observation of the fibrosis and/or prefibrogenic injury is consistent with early injury (Ghosh and Vaughan, 2012). For example, ECM production is counterbalanced by the matrix metalloproteinases encoded by *Mmp2* and *Mmp9* and their negative regulators, the tissue inhibitors of metalloproteinases (TIMPs) (Kim *et al.*, 2010; Van Wettere *et al.*, 2013). *Timp1* (but not *Mmp2*) was differentially expressed in this study, a pattern consistent with bias toward early stage, profibrogenic balance. ECM deposition is tightly regulated by the tissue plasminogen and urokinase plasminogen family of proteins (*Plat* and *Plau*) (Croucher *et al.*, 2008; Sokolovic *et al.*, 2013) and their negative regulator, the serpin family plasminogen activator inhibitors (see *Serpine1* and *Serping1*).

ECM-associated genes are elevated in rodent models of compound toxicity and/or *in vitro* models of hepatic stellate cell activation, including the following fibrogenic signature panel genes: (1) *Col1a1* and *Col4a1*, genes encoding collagen isoforms (Chen *et al.*, 2012); (2) *Pcolce* (Collazos and Diaz, 1994; Molleken *et al.*, 2009; Rosenberg *et al.*, 2004); (3) *Arpc1b*, encoding a regulator of actin polymerization (Locatelli *et al.*, 2014); (4) *Anxa2*, a gene associated with fibril formation and fibrinolysis (Locatelli *et al.*, 2014); (5) *Lox*, encoding an enzyme that mediates collagen cross-linking in early fibrosis (Perepelyuk *et al.*, 2013); (6) *Tgln2* (transgelin 2), encoding an ECM synthesis protein (Molleken *et al.*, 2009; Yu *et al.*, 2008); and (7) *Vtn* (vitronectin), encoding a protein serving as a molecular link with the surrounding collagen (Preissner, 1991) (Figure 11). The downregulation of *Vtn* reported here contrasts with reports of *Vtn* elevation in late-stage fibrosis (Koukoulis *et al.*, 2001). Similarly, our study found no change in *Col5a2* or *Fstl1*, regulators of *Col1a1* and *Col2a1*. Protein products of *Vtn* and *Pcolce* were upregulated in the plasma in our study.

Genes regulating the production of myofibroblasts orchestrate epithelial-to-mesenchymal transition, including genes encoding vimentin (*Vim*) and the S100 calcium binding proteins (*S100A11* and -A6) (Xie *et al.*, 2009; Zhai *et al.*, 2014). The calcium binding proteins are associated with liver fibrosis and are targets of the protein encoded by *Tgfb1* (Bjornland *et al.*, 1999;

Komatsu *et al.*, 2000; Mazzucchelli, 2002; Mori *et al.*, 2004; Saleem *et al.*, 2006; Xie *et al.*, 2009; Yingling *et al.*, 2004).

Inflammatory signaling, chemotaxis. Genes encoding adhesion proteins and related mediators of chemotaxis were differentially expressed in response to fibrogenic chemicals, including *Itgal* (Huang and Brigstock, 2011); *Fbn1* (Dubuisson *et al.*, 2001; Lorena *et al.*, 2004); *Lamac2* and its regulator *Lcn2* (*Ngal*), a marker of inflammatory injury and chemotaxis in multiple model systems (Brenner, 2009; Kim *et al.*, 2010; Leung *et al.*, 2012; Seki and Brenner, 2008); and *Vim*, encoding the inflammatory protein VIM (Vassiliadis *et al.*, 2012). Acute phase proteins associated with hepatotoxicity in animal models include *C1qb*, encoding complement component (Cao *et al.*, 2001); *Cp*, encoding the copper-binding ceruloplasmin (negatively correlated with hepatitis B-induced cirrhosis (van Gool *et al.*, 1986); *Gpnmb*, encoding the protein involved in upregulation of restorative macrophages but not profibrotic macrophages (Li *et al.*, 2010); genes encoding the neutrophil-associated chemokines *Cxcl1*, *Cxcl16*, and *Ccl2* (Wald *et al.*, 2004; Xu *et al.*, 2004); *Cd9* and *Cd53*, genes encoding tetraspanin family members associated with hepatic stellate cell migration (Mazzocca *et al.*, 2002; Pinzani and Rombouts, 2004); and the gene encoding the antifibrinolytic protease inhibitor *A2m*. Plasma protein concentration of A2M is currently part of the FibroSure diagnostic panel used clinically to diagnose steatosis and fibrosis (Rossi *et al.*, 2003). The plasma protein concentration of α-2-macroglobulin is elevated in late stage fibrosis; thus, the lack of robust modulation in our study at the gene level is not necessarily inconsistent with the literature. *Lcn2* was the most differentially expressed gene in the signature panel. It is rapidly expressed by injured hepatocytes in response to toxic insult, infection, or inflammation. Studies in *Lcn2*$^{-/-}$ mice suggest that the protein product plays a protective role in returning chemically injured hepatocytes to homeostasis (Borkham-Kamphorst *et al.*, 2013). Cell-cell adhesion markers promote leukocyte infiltration and inflammation at the site of injury, including genes encoding β-1 integrin family members *Itgb2* (Kulkarni *et al.*, 2011), *Lamc2* (Leung *et al.*, 2012), and *Lgals1* and *-3* (Locatelli *et al.*, 2014; Maeda *et al.*, 2003). Interestingly, genes encoding major histocompatibility complex proteins are also reported to be differentially expressed in response to toxic insults in the liver (*Rt1-da, RT1-dma* (Jimenez *et al.*, 2002; Peterson *et al.*, 2002). The protein product of *Cp* was upregulated in the plasma in our study, and interaction analysis specificity for the fibrosis phenotype.

Other. Upregulation of genes encoding contractility proteins such as *Pkm2* and *Slc25a4* is consistent with energy crisis in fibrotic or necrotic tissue (Chen *et al.*, 2012). Differential regulation of genes in the cytochrome P450 family (*Cyba and Cyp2c11*) is consistent with alterations in xenobiotic metabolism genes in response to hepatotoxins (Chan *et al.*, 2012). However, the lack of modulation in mitochondrial superoxide 2 (*Sod2*) is unexpected, given the role of the protein product in mitochondrial oxidative stress (Lee *et al.*, 2013). Differentially upregulated genes without previous literature-based association with fibrotic, cirrhotic, or hepatotoxic injury include *Fam102b* and *Fam105a*. *Fam102b* is an estrogen-responsive gene that modulates osteoclastogenesis in bone remodeling and repair (Choi *et al.*, 2013). The presented research could suggest a novel role for these genes in the pathogenesis of fibrosis and/or bile duct hyperplasia.

In summary, although not all of the genes in the panel have been directly associated with liver fibrosis previously, all genes have been associated to some extent with cirrhotic and/or fibrotic mechanisms or with processes in the cascade of events leading to fibrosis and/or cirrhosis.

Study Limitations

This study is limited by the small number of chemicals used to validate the gene signature and the overlap in pathogenic processes as identified using light microscopy: the fibrotic phenotype was comorbid with hepatocellular necrosis and bile duct hyperplasia, although bile duct hyperplasia and fibrosis often occur concurrently, and bile duct hyperplasia may precede fibrosis. Furthermore, the gene signatures were originally based on microscopic diagnosis of fibrosis, a more advanced progression of the formation of scar tissue following cell death. We are currently evaluating the prognostic value of the gene signature panel to diagnose fibrosis before histopathologic lesions are evident (ie, 1 day postexposure). The iTRAQ technique used to identify proteins in the serum and plasma is limited by the inability to detect all possible protein products due to the large dynamic range of proteins in the blood (Anderson and Anderson, 2002). Using novel nondestructive extraction methods, ongoing studies related to this research are evaluating the gene signature panel on tissue directly extracted from the regions of injury compared with uninjured areas within the same tissue slide. Body weight loss of 25% is the minimum threshold for wasting syndrome; animals at the higher dose ranges have experienced changes in liver metabolism and physiology secondary to pathological weight loss (Viluksela *et al.*, 1997a,b, 1998a,b, 1999). The fibrotic phenotype observed microscopically was used to link the gene responses but the animals dosed with allyl alcohol did not consistently develop fibrosis. Inference of protein expression patterns cannot be directly made from gene expression data. The greatest utility of a diagnostic test is in the expressed proteins or metabolites in an accessible biofluid (eg, plasma, urine, saliva), rather than gene expression in the injured tissue, accessible only by liver biopsy. In one instance (fibronectin), the liver gene, plasma protein, and tissue protein expression data were discordant. We do not have definitive data providing rationale for the difference in direction for the fibronectin precursor at the gene and protein level. However, our data indicate that the expression of fibronectin is elevated in the tissue but reduced relative to controls in the plasma. Plasma fibronectin can be bound and assembled in the tissue (To *et al.*, 2011). It is possible that the lower gene expression in plasma and corresponding increase in the tissue is a result of plasma fibronectin recruitment to the liver tissue. The gene expression data support an increase in expression of liver fibronectin. This supposition is corroborated by the tissue protein data. It is likely that the observed decrease in plasma fibronectin results from increased blood clearance of fibronectin, corresponding to an increase in the tissue.

Despite these limitations, the results of this research allow us to downselect and prioritize candidate targets to develop further in future studies focused on the evaluation of biofluids collected in a longitudinal manner.

CONCLUSIONS

This analysis provides support for using genes in signature panels as bridging biomarkers between the molecular mechanisms and histopathology. The fidelity of the gene signatures with predictions suggests the utility of the bioinformatics approach in determining gene expression patterns linked to phenotype. This approach can complement risk assessment in military and

civilian occupational exposure scenarios by identifying patterns of genes common to multiple drugs and toxins that cause the same liver histopathologies. In the future, such an approach could be applied to clinical decisions related to treatment within the framework of personalized medicine. Our data support moving forward with a panel of at least 54 candidates as early indicators of fibrosis for further development into a predictive biomarker panel. Some of these gene candidates have protein products modulated in the plasma or serum, suggesting that further research may refine the gene panels into complementary protein panels for developing minimally invasive screening strategies.

FUNDING

The work was supported by the Military Operational Medicine Research Program and the U.S. Army's Network Science Initiative, U.S. Army Medical Research and Materiel Command, Fort Detrick, Maryland. This work was also supported in part by an appointment at U.S. Army Center for Environmental Health Research administered by Oak Ridge Institute for Science and Education through an interagency agreement between U.S. Department of Energy and U.S. Army Medical Research and Materiel Command [B.C.M.].

ACKNOWLEDGMENTS

The authors gratefully acknowledge programmatic support from COL Thomas C. Timmes, USA, Commander of United States Army Center for Environmental Health Research (USACEHR) and the staff of Integrated Laboratory Systems, Inc. The views, opinions, assertions, and/or findings contained herein are those of the authors and should not be construed as official U.S. Department of Defense or Department of the Army position, policy, or decision, unless so designated by other official documentation. Citations of commercial organizations or trade names in this report do not constitute an official Department of the Army endorsement or approval of the products or services of these organizations. This paper has been approved for public release with unlimited distribution.

SUPPLEMENTARY DATA

Supplementary data are available online at http://toxsci.oxfordjournals.org/.

REFERENCES

AbdulHameed, M. D., Tawa, G. J., Kumar, K., Ippolito, D. L., Lewis, J. A., Stallings, J. D., and Wallqvist, A. (2014). Systems level analysis and identification of pathways and networks associated with liver fibrosis. *PLoS One* **9**, e112193.

Ahn, J. M., Sung, H. J., Yoon, Y. H., Kim, B. G., Yang, W. S., Lee, C., Park, H. M., Kim, B. J., Kim, B. G., Lee, S. Y., *et al.* (2014). Integrated glycoproteomics demonstrates fucosylated serum paraoxonase 1 alterations in small cell lung cancer. *Mol. Cell. Proteomics* **13**, 30–48.

Alcaraz, N., Friedrich, T., Kotzing, T., Krohmer, A., Muller, J., Pauling, J., and Baumbach, J. (2012). Efficient key pathway mining: Combining networks and OMICS data. *Integr. Biol.* **4**, 756–764.

Aldridge, J. E., Gibbons, J. A., Flaherty, M. M., Kreider, M. L., Romano, J. A., and Levin, E. D. (2003). Heterogeneity of toxicant response: Sources of human variability. *Toxicol. Sci.* **76**, 3–20.

Alfirevic, A., and Pirmohamed, M. (2012). Predictive genetic testing for drug-induced liver injury: Considerations of clinical utility. *Clin. Pharmacol. Ther.* **92**, 376–380.

Allen, J.H. (2013). The wicked problem of chemicals policy: Opportunities for innovation. *J. Environ. Stud. Sci.* **3**, 101–108.

Alpini, G., Lenzi, R., Sarkozi, L., and Tavoloni, N. (1988). Biliary physiology in rats with bile ductular cell hyperplasia. Evidence for a secretory function of proliferated bile ductules. *J. Clin. Invest.* **81**, 569–578.

Amacher, D. E. (2010). The discovery and development of proteomic safety biomarkers for the detection of drug-induced liver toxicity. *Toxicol. Appl. Pharmacol.* **245**, 134–142.

Anderson, N. L., and Anderson, N. G. (2002). The human plasma proteome: History, character, and diagnostic prospects. *Mol. Cell. Proteomics* **1**, 845–867.

Antoine, D. J., Dear, J. W., Lewis, P. S., Platt, V., Coyle, J., Masson, M., Thanacoody, R. H., Gray, A. J., Webb, D. J., Moggs, J. G., *et al.* (2013). Mechanistic biomarkers provide early and sensitive detection of acetaminophen-induced acute liver injury at first presentation to hospital. *Hepatology* **58**, 777–787.

Baranova, A., Lal, P., Birerdinc, A., and Younossi, Z. M. (2011). Non-invasive markers for hepatic fibrosis. *BMC Gastroenterol.* **11**, 91.

Bataller, R., and Brenner, D. A. (2005). Liver fibrosis. *J. Clin. Invest.* **115**, 209–218.

Beger, R. D., Sun, J., and Schnackenberg, L. K. (2010). Metabolomics approaches for discovering biomarkers of drug-induced hepatotoxicity and nephrotoxicity. *Toxicol. Appl. Pharmacol.* **243**, 154–166.

Bjornland, K., Winberg, J. O., Odegaard, O. T., Hovig, E., Loennechen, T., Aasen, A. O., Fodstad, O., and Maelandsmo, G. M. (1999). S100A4 involvement in metastasis: Deregulation of matrix metalloproteinases and tissue inhibitors of matrix metalloproteinases in osteosarcoma cells transfected with an anti-S100A4 ribozyme. *Cancer Res.* **59**, 4702–4708.

Borkham-Kamphorst, E., van de Leur, E., Zimmermann, H. W., Karlmark, K. R., Tihaa, L., Haas, U., Tacke, F., Berger, T., Mak, T. W., and Weiskirchen, R. (2013). Protective effects of lipocalin-2 (LCN2) in acute liver injury suggest a novel function in liver homeostasis. *Biochim. Biophys. Acta* **1832**, 660–673.

Breitling, R., Armengaud, P., Amtmann, A., and Herzyk, P. (2004). Rank products: A simple, yet powerful, new method to detect differentially regulated genes in replicated microarray experiments. *FEBS Lett.* **573**, 83–92.

Brenner, D. A. (2009). Molecular pathogenesis of liver fibrosis. *Trans. Am. Clin. Climatol. Assoc.* **120**, 361–368.

Campion, S., Aubrecht, J., Boekelheide, K., Brewster, D. W., Vaidya, V. S., Anderson, L., Burt, D., Dere, E., Hwang, K., Pacheco, S., *et al.* (2013). The current status of biomarkers for predicting toxicity. *Expert opin. Drug Metab Toxicol.* **9**, 1391–1408.

Cao, S. X., Dhahbi, J. M., Mote, P. L., and Spindler, S. R. (2001). Genomic profiling of short- and long-term caloric restriction effects in the liver of aging mice. *Proc. Natl. Acad. Sci. U.S.A.* **98**, 10630–10635.

Causey, M. W., Salgar, S., Singh, N., Martin, M., and Stallings, J. D. (2012). Valproic acid reversed pathologic endothelial cell gene expression profile associated with ischemia-reperfusion injury in a swine hemorrhagic shock model. *J. Vasc. Surg.* **55**, 1096–1103 e51.

Chan, J., Sharkey, F. E., Kushwaha, R. S., VandeBerg, J. F., and VandeBerg, J. L. (2012). Steatohepatitis in laboratory opossums exhibiting a high lipemic response to dietary cholesterol and fat. *Am. J. Physiol. Gastrointest. Liver Physiol.* **303**, G12–G19.

Chen, J. W., Nielsen, M. F., Caumo, A., Vilstrup, H., Christiansen, J. S., and Frystyk, J. (2006). Changes in bioactive IGF-I and IGF-binding protein-1 during an oral glucose tolerance test in patients with liver cirrhosis. *Eur. J. Endocrinol.* **155**, 285–292.

Chen, M., David, C. J., and Manley, J. L. (2012). Concentration-dependent control of pyruvate kinase M mutually exclusive splicing by hnRNP proteins. *Nat. Struct. Mol. Biol.* **19**, 346–354.

Choi, H. K., Kang, H. R., Jung, E., Kim, T. E., Lin, J. J., and Lee, S. Y. (2013). Early estrogen-induced gene 1, a novel RANK signaling component, is essential for osteoclastogenesis. *Cell Res.* **23**, 524–536.

Coiro, V., and Goodman, H. M. (1987). Pituitary secretions related to adrenocorticotropic hormone induce sensitivity of adipose tissue to the insulin-like actions of growth hormone. *Neuroendocrinology* **45**, 165–171.

Collazos, J., and Diaz, F. (1994). Procollagen-III peptide concentrations in serum of patients with chronic active hepatitis compared with mild hepatic disorders. *Clin. Biochem.* **27**, 189–191.

Croucher, D. R., Saunders, D. N., Lobov, S., and Ranson, M. (2008). Revisiting the biological roles of PAI2 (SERPINB2) in cancer. *Nat. Rev. Cancer* **8**, 535–545.

Cui, S., EauClaire, S. F., and Matthews, R. P. (2013). Interferon-gamma directly mediates developmental biliary defects. *Zebrafish* **10**, 177–183.

Cui, Y., and Paules, R. S. (2010). Use of transcriptomics in understanding mechanisms of drug-induced toxicity. *Pharmacogenomics* **11**, 573–585.

Dalmas, D. A., Scicchitano, M. S., Mullins, D., Hughes-Earle, A., Tatsuoka, K., Magid-Slav, M., Frazier, K. S., and Thomas, H. C. (2011). Potential candidate genomic biomarkers of drug induced vascular injury in the rat. *Toxicol. Appl. Pharmacol.* **257**, 284–300.

Davis, R. A., Kern, F., Jr, Showalter, R., Sutherland, E., Sinensky, M., and Simon, F. R. (1978). Alterations of hepatic Na+,K+-atpase and bile flow by estrogen: Effects on liver surface membrane lipid structure and function. *Proc. Natl. Acad. Sci. U.S.A.* **75**, 4130–4134.

Despa, S., Bossuyt, J., Han, F., Ginsburg, K. S., Jia, L. G., Kutchai, H., Tucker, A. L., and Bers, D. M. (2005). Phospholemman-phosphorylation mediates the beta-adrenergic effects on Na/K pump function in cardiac myocytes. *Circ. Res.* **97**, 252–259.

Dubuisson, L., Lepreux, S., Bioulac-Sage, P., Balabaud, C., Costa, A. M., Rosenbaum, J., and Desmouliere, A. (2001). Expression and cellular localization of fibrillin-1 in normal and pathological human liver. *J. Hepatol.* **34**, 514–522.

Edginton, A. N., and Willmann, S. (2008). Physiology-based simulations of a pathological condition: Prediction of pharmacokinetics in patients with liver cirrhosis. *Clin. Pharmacokinet.* **47**, 743–752.

Floyd, R. V., Wray, S., Martin-Vasallo, P., and Mobasheri, A. (2010). Differential cellular expression of FXYD1 (phospholemman) and FXYD2 (gamma subunit of Na, K-ATPase) in normal human tissues: A study using high density human tissue microarrays. *Ann. Anat.* **192**, 7–16.

Fontana, R. J. (2014). Pathogenesis of idiosyncratic drug-induced liver injury and clinical perspectives. *Gastroenterology* **146**, 914–928.

Friedman, S. L. (2008). Mechanisms of hepatic fibrogenesis. *Gastroenterology* **134**, 1655–1669.

Fujii, T., Fuchs, B. C., Yamada, S., Lauwers, G. Y., Kulu, Y., Goodwin, J. M., Lanuti, M., and Tanabe, K. K. (2010). Mouse model of carbon tetrachloride induced liver fibrosis: Histopathological changes and expression of CD133 and epidermal growth factor. *BMC Gastroenterol.* **10**, 79.

Ganter, B., Tugendreich, S., Pearson, C. I., Ayanoglu, E., Baumhueter, S., Bostian, K. A., Brady, L., Browne, L. J., Calvin, J. T., Day, G. J., *et al.* (2005). Development of a large-scale chemogenomics database to improve drug candidate selection and to understand mechanisms of chemical toxicity and action. *J. Biotechnol.* **119**, 219–244.

Gentleman, R. C., Carey, V. J., Bates, D. M., Bolstad, B., Dettling, M., Dudoit, S., Ellis, B., Gautier, L., Ge, Y., Gentry, J., *et al.* (2004). Bioconductor: Open software development for computational biology and bioinformatics. *Genome Biol.* **5**, R80.

Ghosh, A. K., and Vaughan, D. E. (2012). PAI-1 in tissue fibrosis. *J. Cell. Physiol.* **227**, 493–507.

Hannivoort, R. A., Hernandez-Gea, V., and Friedman, S. L. (2012). Genomics and proteomics in liver fibrosis and cirrhosis. *Fibrogenesis Tissue Repair* **5**, 1.

Harrill, A. H., and Rusyn, I. (2008). Systems biology and functional genomics approaches for the identification of cellular responses to drug toxicity. *Expert opin. Drug Metab. Toxicol.* **4**, 1379–1389.

Hei, T. K., Zhao, Y., Zhou, H., and Ivanov, V. (2011). Mechanism of radiation carcinogenesis: Role of the TGFBI gene and the inflammatory signaling cascade. *Adv. Exp. Med. Biol.* **720**, 163–170.

Heinloth, A. N., Boorman, G. A., Foley, J. F., Flagler, N. D., and Paules, R. S. (2007). Gene expression analysis offers unique advantages to histopathology in liver biopsy evaluations. *Toxicol. Pathol.* **35**, 276–283.

Huang, G., and Brigstock, D. R. (2011). Integrin expression and function in the response of primary culture hepatic stellate cells to connective tissue growth factor (CCN2). *J. Cell. Mol. Med.* **15**, 1087–1095.

Igarashi, Y., Nakatsu, N., Yamashita, T., Ono, A., Ohno, Y., Urushidani, T., and Yamada, H. (2015). Open TG-GATEs: A large-scale toxicogenomics database. *Nucleic Acids Res.* **43**(Database issue), D921–D927.

Ihmels, J., Friedlander, G., Bergmann, S., Sarig, O., Ziv, Y., and Barkai, N. (2002). Revealing modular organization in the yeast transcriptional network. *Nat. Genet.* **31**, 370–377.

Institute of Laboratory Animal Resources. (2011). *Guide for the Care and Use of Laboratory Animals*. National Academies Press (US), Washington, D.C.

Irwin, R. D. (2006). NTP Technical Report on the comparative toxicity studies of allyl acetate (CAS No. 591-87-7), allyl alcohol (CAS No. 107-18-6) and acrolein (CAS No. 107-02-8) administered by gavage to F344/N rats and B6C3F1 mice. *Toxic. Rep. Ser.***48**, 1–73, A1-H10.

Jackson, E. R., Kilroy, C., Joslin, D. L., Schomaker, S. J., Pruimboom-Brees, I., and Amacher, D. E. (2008). The early effects of short-term dexamethasone administration on hepatic and serum alanine aminotransferase in the rat. *Drug Chem. Toxicol.* **31**, 427–445.

Jaeschke, H., Kleinwaechter, C., and Wendel, A. (1987). The role of acrolein in allyl alcohol-induced lipid peroxidation and liver cell damage in mice. *Biochem. Pharmacol.* **36**, 51–57.

Jimenez, B. D., Maldonado, L., Dahl, R. H., Quattrochi, L. C., and Guzelian, P. S. (2002). Ectopic expression of MHC class II genes (RT1.B(I) beta/alpha) in rat hepatocytes in vivo and in culture can be elicited by treatment with the pregnane X

receptor agonists pregnenolone 16 alpha-carbonitrile and dexamethasone. *Life Sci.* **71**, 311–323.

Joliffe, I. T., and Morgan, B. J. (1992). Principal component analysis and exploratory factor analysis. *Stat. Methods Med. Res.* **1**, 69–95.

Jung, S. A., Chung, Y. H., Park, N. H., Lee, S. S., Kim, J. A., Yang, S. H., Song, I. H., Lee, Y. S., Suh, D. J., and Moon, I. H. (2000). Experimental model of hepatic fibrosis following repeated periportal necrosis induced by allylalcohol. *Scand. J. Gastroenterol.* **35**, 969–975.

Kamada, Y., Tamura, S., Kiso, S., Matsumoto, H., Saji, Y., Yoshida, Y., Fukui, K., Maeda, N., Nishizawa, H., Nagaretani, H., *et al.* (2003). Enhanced carbon tetrachloride-induced liver fibrosis in mice lacking adiponectin. *Gastroenterology* **125**, 1796–1807.

Kim, J. W., Lee, S. H., Jeong, S. H., Kim, H., Ahn, K. S., Cho, J. Y., Yoon, Y. S., and Han, H. S. (2010). Increased urinary lipocalin-2 reflects matrix metalloproteinase-9 activity in chronic hepatitis C with hepatic fibrosis. *Tohoku J. Exp. Med.* **222**, 319–327.

Komatsu, K., Kobune-Fujiwara, Y., Andoh, A., Ishiguro, S., Hunai, H., Suzuki, N., Kameyama, M., Murata, K., Miyoshi, J., Akedo, H., *et al.* (2000). Increased expression of S100A6 at the invading fronts of the primary lesion and liver metastasis in patients with colorectal adenocarcinoma. *Br. J. Cancer* **83**, 769–774.

Koukoulis, G. K., Shen, J., Virtanen, I., and Gould, V. E. (2001). Vitronectin in the cirrhotic liver: An immunomarker of mature fibrosis. *Hum. Pathol.* **32**, 1356–1362.

Kulkarni, A. A., Thatcher, T. H., Olsen, K. C., Maggirwar, S. B., Phipps, R. P., and Sime, P. J. (2011). PPAR-gamma ligands repress TGFbeta-induced myofibroblast differentiation by targeting the PI3K/Akt pathway: Implications for therapy of fibrosis. *PLoS One* **6**, e15909.

Lahaye, P., Tazi, K. A., Rona, J. P., Dellis, O., Lebrec, D., and Moreau, R. (1998). Effects of protein kinase C modulators on Na+/K+ adenosine triphosphatase activity and phosphorylation in aortae from rats with cirrhosis. *Hepatology* **28**, 663–669.

Lee, Y. H., Goh, W. W., Ng, C. K., Raida, M., Wong, L., Lin, Q., Boelsterli, U. A., and Chung, M. C. (2013). Integrative toxicoproteomics implicates impaired mitochondrial glutathione import as an off-target effect of troglitazone. *J. Proteome Res.* **12**, 2933–2945.

Lertratanangkoon, K., Horning, E. C., and Horning, M. G. (1993). Pathways of formation of 2-, 3- and 4-bromophenol from bromobenzene. Proposed mechanism for C-S lyase reactions of cysteine conjugates. *Res. Commun. Chem. Pathol. Pharmacol.* **80**, 259–282.

Leung, L., Radulovich, N., Zhu, C. Q., Organ, S., Bandarchi, B., Pintilie, M., To, C., Panchal, D., and Tsao, M. S. (2012). Lipocalin2 promotes invasion, tumorigenicity and gemcitabine resistance in pancreatic ductal adenocarcinoma. *PLoS One* **7**, e46677.

Li, B., Castano, A. P., Hudson, T. E., Nowlin, B. T., Lin, S. L., Bonventre, J. V., Swanson, K. D., and Duffield, J. S. (2010). The melanoma-associated transmembrane glycoprotein Gpnmb controls trafficking of cellular debris for degradation and is essential for tissue repair. *FASEB J* **24**, 4767–4781.

Liu, R. M. (2008). Oxidative stress, plasminogen activator inhibitor 1, and lung fibrosis. *Antioxid. Redox Signal.* **10**, 303–319.

Liu, R. M., Choi, J., Wu, J. H., Gaston Pravia, K. A., Lewis, K. M., Brand, J. D., Mochel, N. S., Krzywanski, D. M., Lambeth, J. D., Hagood, J. S., *et al.* (2010). Oxidative modification of nuclear mitogen-activated protein kinase phosphatase 1 is involved in transforming growth factor beta1-induced expression of plasminogen activator inhibitor 1 in fibroblasts. *J. Biol. Chem.* **285**, 16239–16247.

Liu, R. M., and Gaston Pravia, K. A. (2010). Oxidative stress and glutathione in TGF-beta-mediated fibrogenesis. *Free Radic. Biol. Med.* **48**, 1–15.

Locatelli, I., Sutti, S., Jindal, A., Vacchiano, M., Bozzola, C., Reutelingsperger, C., Kusters, D., Bena, S., Parola, M., Paternostro, C., *et al.* (2014). Endogenous annexin A1 is a novel protective determinant in nonalcoholic steatohepatitis in mice. *Hepatology* **60**, 531–544.

Lorena, D., Darby, I. A., Reinhardt, D. P., Sapin, V., Rosenbaum, J., and Desmouliere, A. (2004). Fibrillin-1 expression in normal and fibrotic rat liver and in cultured hepatic fibroblastic cells: Modulation by mechanical stress and role in cell adhesion. *Lab. Invest.* **84**, 203–212.

Lu, Y. Y., Chen, Q. L., Guan, Y., Guo, Z. Z., Zhang, H., Zhang, W., Hu, Y. Y., and Su, S. B. (2014). Transcriptional profiling and co-expression network analysis identifies potential biomarkers to differentiate chronic hepatitis B and the caused cirrhosis. *Mol. Biosyst.* **10**, 1117–1125.

Lupp, A., Lucas, N., Lindstrom-Seppa, P., Koponen, K., Hanninen, O., Danz, M., and Klinger, W. (1998). Transplantation of fetal liver tissue suspension into the spleens of adult syngenic rats: Effects of beta-naphthoflavone, phenobarbital and dexamethasone on cytochrome P450 isoforms expression and on glycogen storage. *Exp. Toxicol. Pathol.* **50**, 173–183.

Maeda, N., Kawada, N., Seki, S., Arakawa, T., Ikeda, K., Iwao, H., Okuyama, H., Hirabayashi, J., Kasai, K., and Yoshizato, K. (2003). Stimulation of proliferation of rat hepatic stellate cells by galectin-1 and galectin-3 through different intracellular signaling pathways. *J. Biol. Chem.* **278**, 18938–18944.

Massague, J., and Gomis, R. R. (2006). The logic of TGFbeta signaling. *FEBS Lett.* **580**, 2811–2820.

Mazzocca, A., Carloni, V., Sciammetta, S., Cordella, C., Pantaleo, P., Caldini, A., Gentilini, P., and Pinzani, M. (2002). Expression of transmembrane 4 superfamily (TM4SF) proteins and their role in hepatic stellate cell motility and wound healing migration. *J. Hepatol.* **37**, 322–330.

Mazzucchelli, L. (2002). Protein S100A4: Too long overlooked by pathologists? *Am. J. Pathol.* **160**, 7–13.

Meldrum, C., Doyle, M. A., and Tothill, R. W. (2011). Next-generation sequencing for cancer diagnostics: A practical perspective. *Clin. Biochem. Rev.* **32**, 177–195.

Molleken, C., Sitek, B., Henkel, C., Poschmann, G., Sipos, B., Wiese, S., Warscheid, B., Broelsch, C., Reiser, M., Friedman, S. L., *et al.* (2009). Detection of novel biomarkers of liver cirrhosis by proteomic analysis. *Hepatology* **49**, 1257–1266.

Mori, M., Shimada, H., Gunji, Y., Matsubara, H., Hayashi, H., Nimura, Y., Kato, M., Takiguchi, M., Ochiai, T., and Seki, N. (2004). S100A11 gene identified by in-house cDNA microarray as an accurate predictor of lymph node metastases of gastric cancer. *Oncol. Rep.* **11**, 1287–1293.

Moustafa, S. A. (2001). Effect of glutathione (GSH) depletion on the serum levels of triiodothyronine (T3), thyroxine (T4), and T3/T4 ratio in allyl alcohol-treated male rats and possible protection with zinc. *Int. J. Toxicol.* **20**, 15–20.

Nakken, K. E., Nygard, S., Haaland, T., Berge, K. E., Arnkvaern, K., Odegaard, A., Labori, K. J., and Raeder, M. G. (2007). Multiple inflammatory-, tissue remodelling- and fibrosis genes are differentially transcribed in the livers of Abcb4 (-/ -) mice harbouring chronic cholangitis. *Scand. J. Gastroenterol.* **42**, 1245–1255.

National Toxicology Program. (2002). 4, 4′-Methylenedianiline and its dihydrochloride salt. *Rep. Carcinog.* **10**, 152–153.

National Toxicology Program. (2010). DrugMatrix®. Available at: https://ntp.niehs.nih.gov/drugmatrix/index.html. Accessed 4 September 2015.

National Toxicology Program. (2011). Carbon tetrachloride. *Rep. Carcinog.* **12**, 86–89.

Nesvizhskii, A. I., Keller, A., Kolker, E., and Aebersold, R. (2003). A statistical model for identifying proteins by tandem mass spectrometry. *Anal. Chem.* **75**, 4646–4658.

Novosyadlyy, R., Dargel, R., and Scharf, J. G. (2005). Expression of insulin-like growth factor-I and insulin-like growth factor binding proteins during thioacetamide-induced liver cirrhosis in rats. *Growth Horm. IGF Res.* **15**, 313–323.

Ozer, J., Ratner, M., Shaw, M., Bailey, W., and Schomaker, S. (2008). The current state of serum biomarkers of hepatotoxicity. *Toxicology* **245**, 194–205.

Perepelyuk, M., Terajima, M., Wang, A. Y., Georges, P. C., Janmey, P. A., Yamauchi, M., and Wells, R. G. (2013). Hepatic stellate cells and portal fibroblasts are the major cellular sources of collagens and lysyl oxidases in normal liver and early after injury. *Am. J. Physiol. Gastrointest. Liver Physiol.* **304**, G605–G614.

Peterson, R. L., Wang, L., Albert, L., Marchese, E., Erickson, J., Wong, A., Mounts, W. M., Hayes, L., Bouchard, P., Keith, J., *et al.* (2002). Pharmacogenomic analysis of rhIL-11 treatment in the HLA-B27 rat model of inflammatory bowel disease. *Pharmacogenomics J.* **2**, 383–399.

Pinzani, M., and Rombouts, K. (2004). Liver fibrosis: From the bench to clinical targets. *Dig. Liver Dis.* **36**, 231–242.

Preissner, K. T. (1991). Structure and biological role of vitronectin. *Annu. Rev. Cell Biol.* **7**, 275–310.

Qu, Y., He, F., and Chen, Y. (2010). Different effects of the probe summarization algorithms PLIER and RMA on high-level analysis of Affymetrix exon arrays. *BMC Bioinformatics* **11**, 211.

Reiner, A., Yekutieli, D., and Benjamini, Y. (2003). Identifying differentially expressed genes using false discovery rate controlling procedures. *Bioinformatics* **19**, 368–375.

Rosenberg, W. M., Voelker, M., Thiel, R., Becka, M., Burt, A., Schuppan, D., Hubscher, S., Roskams, T., Pinzani, M., Arthur, M. J., *et al.* (2004). Serum markers detect the presence of liver fibrosis: A cohort study. *Gastroenterology* **127**, 1704–1713.

Ross, R. J., Chew, S. L., D'Souza Li, L., Yateman, M., Rodriguez-Arnao, J., Gimson, A., Holly, J., and Camacho-Hubner, C. (1996). Expression of IGF-I and IGF-binding protein genes in cirrhotic liver. *J. Endocrinol.* **149**, 209–216.

Rossi, E., Adams, L., Prins, A., Bulsara, M., de Boer, B., Garas, G., MacQuillan, G., Speers, D., and Jeffrey, G. (2003). Validation of the FibroTest biochemical markers score in assessing liver fibrosis in hepatitis C patients. *Clin. Chem.* **49**, 450–454.

Saleem, M., Kweon, M. H., Johnson, J. J., Adhami, V. M., Elcheva, I., Khan, N., Bin Hafeez, B., Bhat, K. M., Sarfaraz, S., Reagan-Shaw, S., *et al.* (2006). S100A4 accelerates tumorigenesis and invasion of human prostate cancer through the transcriptional regulation of matrix metalloproteinase 9. *Proc. Natl. Acad. Sci. U.S.A.* **103**, 14825–14830.

Seki, E., and Brenner, D. A. (2008). Toll-like receptors and adaptor molecules in liver disease: Update. *Hepatology* **48**, 322–335.

Shadforth, I. P., Dunkley, T. P., Lilley, K. S., and Bessant, C. (2005). i-Tracker: For quantitative proteomics using iTRAQ. *BMC Genomics* **6**, 145.

Smialowicz, R. J., Simmons, J. E., Luebke, R. W., and Allis, J. W. (1991). Immunotoxicologic assessment of subacute exposure of rats to carbon tetrachloride with comparison to hepatotoxicity and nephrotoxicity. *Fundam. Appl. Toxicol.* **17**, 186–196.

Sokolovic, A., van Roomen, C. P., Ottenhoff, R., Scheij, S., Hiralall, J. K., Claessen, N., Aten, J., Oude Elferink, R. P., Groen, A. K., and Sokolovic, M. (2013). Fasting reduces liver fibrosis in a mouse model for chronic cholangiopathies. *Biochim. Biophys. Acta* **1832**, 1482–1491.

Tawa, G. J., AbdulHameed, M.D.M., Yu, X., Kumar, K., Ippolito, D. L., Lewis, J. A., Stallings, J. D., Reifman, J., and Wallqvist, A. (2014). Characterization of chemically induced liver injuries using gene co-expression modules. *PLoS One* **9**, e107230.

Thoolen, B., Maronpot, R. R., Harada, T., Nyska, A., Rousseaux, C., Nolte, T., Malarkey, D. E., Kaufmann, W., Kuttler, K., Deschl, U., *et al.* (2010). Proliferative and nonproliferative lesions of the rat and mouse hepatobiliary system. *Toxicol. Pathol.* **38**(7 Suppl.), 5S–81S.

To, W.S., and Midwood, K.S. (2011). Plasma and cellular fibronectin: Distinct independent functions during tissue repair. *Fibrogenesis Tissue Repair* **4**,1–17.

Ueberham, E., Low, R., Ueberham, U., Schonig, K., Bujard, H., and Gebhardt, R. (2003). Conditional tetracycline-regulated expression of TGF-beta1 in liver of transgenic mice leads to reversible intermediary fibrosis. *Hepatology* **37**, 1067–1078.

van Gool, J., de Nie, I., Smit, J., and Zuyderhoudt, F. M. (1986). Mechanisms by which acute phase proteins enhance development of liver fibrosis: Effects on collagenase and prolyl-4-hydroxylase activity in the rat liver. *Exp. Mol. Pathol.* **45**, 160–170.

Van Wettere, A. J., Law, J. M., Hinton, D. E., and Kullman, S. W. (2013). Anchoring hepatic gene expression with development of fibrosis and neoplasia in a toxicant-induced fish model of liver injury. *Toxicol. Pathol.* **41**, 744–760.

Vandesompele, J., De Preter, K., Pattyn, F., Poppe, B., Van Roy, N., De Paepe, A., and Speleman, F. (2002). Accurate normalization of real-time quantitative RT-PCR data by geometric averaging of multiple internal control genes. *Genome Biol.* **3**, RESEARCH0034.

Vassiliadis, E., Oliveira, C. P., Alvares-da-Silva, M. R., Zhang, C., Carrilho, F. J., Stefano, J. T., Rabelo, F., Pereira, L., Kappel, C. R., Henriksen, K., *et al.* (2012). Circulating levels of citrullinated and MMP-degraded vimentin (VICM) in liver fibrosis related pathology. *Am. J. Transl. Res.* **4**, 403–414.

Viluksela, M., Stahl, B. U., Birnbaum, L. S., and Rozman, K. K. (1997a). Subchronic/chronic toxicity of 1,2,3,4,6,7,8-hepta chlorodibenzo-p-dioxin (HpCDD) in rats. Part II. Biochemical effects. *Toxicol. Appl. Pharmacol* **146**, 217–226.

Viluksela, M., Stahl, B. U., Birnbaum, L. S., and Rozman, K. K. (1998a). Subchronic/chronic toxicity of a mixture of four chlorinated dibenzo-p-dioxins in rats. II. Biochemical effects. *Toxicol. Appl. Pharmacol.* **151**, 70–78.

Viluksela, M., Stahl, B. U., Birnbaum, L. S., Schramm, K. W., Kettrup, A., and Rozman, K. K. (1997b). Subchronic/chronic toxicity of 1,2,3,4,6,7,8-heptachlorodibenzo-p-dioxin (HpCDD) in rats. Part I. Design, general observations, hematology, and liver concentrations. *Toxicol. Appl. Pharmacol.* **146**, 207–216.

Viluksela, M., Stahl, B. U., Birnbaum, L. S., Schramm, K. W., Kettrup, A., and Rozman, K. K. (1998b). Subchronic/chronic toxicity of a mixture of four chlorinated dibenzo-p-dioxins in rats. I. Design, general observations, hematology,and liver concentrations. *Toxicol. Appl. Pharmacol.* **151**, 57–69.

Viluksela, M., Unkila, M., Pohjanvirta, R., Tuomisto, J. T., Stahl, B. U., Rozman, K. K., and Tuomisto, J. (1999). Effects of 2,3,7,8-tetrachlorodibenzo-p-dioxin (TCDD) on liver phosphoenolpyruvate carboxykinase (PEPCK) activity, glucose homeostasis and plasma amino acid concentrations in the

most TCDD-susceptible and the most TCDD-resistant rat strains. *Arch. Toxicol.* **73**, 323–336.

Vinken, M. (2013). The adverse outcome pathway concept: A pragmatic tool in toxicology. *Toxicology* **312**, 158–165.

Wald, O., Pappo, O., Safadi, R., Dagan-Berger, M., Beider, K., Wald, H., Franitza, S., Weiss, I., Avniel, S., Boaz, P., *et al.* (2004). Involvement of the CXCL12/CXCR4 pathway in the advanced liver disease that is associated with hepatitis C virus or hepatitis B virus. *Eur. J. Immunol.* **34**, 1164–1174.

Weber, L. W., Boll, M., and Stampfl, A. (2003). Hepatotoxicity and mechanism of action of haloalkanes: Carbon tetrachloride as a toxicological model. *Crit. Rev. Toxicol.* **33**, 105–136.

Xie, R., Schlumbrecht, M. P., Shipley, G. L., Xie, S., Bassett, R. L., Jr, and Broaddus, R. R. (2009). S100A4 mediates endometrial cancer invasion and is a target of TGF-beta1 signaling. *Lab. Invest.* **89**, 937–947.

Xu, J., Lee, G., Wang, H., Vierling, J. M., and Maher, J. J. (2004). Limited role for CXC chemokines in the pathogenesis of alpha-naphthylisothiocyanate-induced liver injury. *Am. J. Physiol. Gastrointest. Liver Physiol.* **287**, G734–G741.

Yingling, J. M., Blanchard, K. L., and Sawyer, J. S. (2004). Development of TGF-beta signalling inhibitors for cancer therapy. *Nat. Rev. Drug Discov.* **3**, 1011–1022.

Yu, C., Wang, F., Jin, C., Wu, X., Chan, W. K., and McKeehan, W. L. (2002). Increased carbon tetrachloride-induced liver injury and fibrosis in FGFR4-deficient mice. *Am. J. Pathol.* **161**, 2003–2010.

Yu, H., Konigshoff, M., Jayachandran, A., Handley, D., Seeger, W., Kaminski, N., and Eickelberg, O. (2008). Transgelin is a direct target of TGF-beta/Smad3-dependent epithelial cell migration in lung fibrosis. *FASEB J.* **22**, 1778–1789.

Yu, H. Y., Wang, B. L., Zhao, J., Yao, X. M., Gu, Y., and Li, Y. (2009). Protective effect of bicyclol on tetracycline-induced fatty liver in mice. *Toxicology* **261**, 112–118.

Zhai, X., Zhu, H., Wang, W., Zhang, S., Zhang, Y., and Mao, G. (2014). Abnormal expression of EMT-related proteins, S100A4, vimentin and E-cadherin, is correlated with clinicopathological features and prognosis in HCC. *Med. Oncol.* **31**, 970.

Zhang, J. D., Berntenis, N., Roth, A., and Ebeling, M. (2014). Data mining reveals a network of early-response genes as a consensus signature of drug-induced in vitro and in vivo toxicity. *Pharmacogenomics J.* **14**, 208–216.

Zhang, X., Lambert, J. C., Doll, M. A., Walraven, J. M., Arteel, G. E., and Hein, D. W. (2006). 4,4′-methylenedianiline-induced hepatotoxicity is modified by N-acetyltransferase 2 (NAT2) acetylator polymorphism in the rat. *J. Pharmacol. Exp. Ther.* **316**, 289–294.

Zhao, C., Dai, C. L., Xu, F., Ju, X. H., Li, X. D., and Wang, C. Y. (2008). [Patterns of hepatic cells death during hepatic ischemia/reperfusion injury in cirrhotic rats]. *Zhongguo Yi Xue Ke Xue Yuan Xue Bao* **30**, 455–459.

Zhou, Y., Qin, S., and Wang, K. (2013). Biomarkers of drug-induced liver injury. *Curr. Biomark. Find.* **2013**, 1–9.